Russian Journal of Earth Sciences, Vol. 22, ES6001
https://doi.org/10.2205/2022ES000820

Bjerknes compensation mechanism as a possible trigger of the low-frequency variability of Arctic amplification

Mikhail M. Latonin*[,1,2], Igor L. Bashmachnikov[1,2], and Leonid P. Bobylev[1]

[1] *Nansen International Environmental and Remote Sensing Centre, 14th Line 7, Vasilievsky Island, 199034 Saint Petersburg, Russia*
[2] *Saint Petersburg State University, Universitetskaya Emb. 7–9, 199034 Saint Petersburg, Russia*

Received 19 August 2022; accepted 7 November 2022; published 22 November 2022.

The causes of Arctic amplification are widely debated, and a cohesive picture has not been obtained yet. This study has investigated the role of the Atlantic meridional oceanic and atmospheric heat transport into the Arctic in the emergence of Arctic amplification. The integral advective fluxes in the layer of Atlantic waters and in the lower troposphere were considered. The results show a strong coupling between the meridional heat fluxes and regional Arctic amplification in the Eurasian Arctic on the decadal time scales (10–15 years). We argue that the low-frequency variability of Arctic amplification is regulated via the chain of oceanic heat transport – atmospheric heat transport – Arctic amplification. The atmospheric response to the ocean influence occurs with a delay of three years and is attributed to the Bjerknes compensation mechanism. In turn, the atmospheric heat and moisture transport directly affects the magnitude of Arctic amplification, with the latter lagging by one year. Thus, the variability of oceanic heat transport at the southern boundary of the Nordic Seas might be a predictor of the Arctic amplification magnitude over the Eurasian Basin of the Arctic Ocean with a lead time of four years. The results are consistent with the concept of the decadal Arctic climate variability expressed via the Arctic Ocean Oscillation index.

Keywords: Oceanic heat transport, Atmospheric heat transport, Decadal variability, Arctic climate, Coupling, Eurasian Basin

Citation: Mikhail M. Latonin, Igor L. Bashmachnikov, and Leonid P. Bobylev (2022), Bjerknes compensation mechanism as a possible trigger of the low-frequency variability of Arctic amplification, *Russian Journal of Earth Sciences*, Vol. 22, ES6001, doi: 10.2205/2022ES000820.

1 Introduction

Present climate change is characterized by an accelerated warming in the Arctic relative to lower latitudes and the global mean [*Allen et al.*, 2018]. This feature has become known as the Arctic amplification of global warming [*Arrhenius*, 1896; *Serreze and Francis*, 2006]. At the same time, Arctic warming is not uniform, with one of the highest current and predicted warming rate over the Russian Arctic [*Volodin et al.*, 2008]. Various mechanisms have been proposed to explain the observed enhancement of the Arctic warming. Several focused review studies have already been published on this highly debated topic [*Serreze and Barry*, 2011; *Latonin et al.*, 2020a; *Previdi et al.*, 2021]. However, there is still no robust evidence on the relative importance of the mechanisms involved. It has been generally accepted that the clearest drivers of Arctic amplification are two temperature feedbacks (Planck feedback and lapse-rate feedback) and surface albedo feedback [*Screen and Simmonds*, 2010; *Graversen et al.*, 2014; *Pithan and Mauritsen*, 2014; *Hwang et al.*, 2018; *Henry and Merlis*, 2019]. There are other important feedbacks too, such as the positive water vapor feedback [*Dessler et al.*, 2008] and both positive and negative cloud feedbacks [*Bony et al.*, 2006]. Nevertheless, there is significant uncertainty in these climate feedbacks as well because of their not completely understood coupling with the atmospheric and oceanic energy transport [*Zelinka and Hartmann*, 2012; *Goosse et al.*, 2018]. Additional complexity arises from the fact that the poleward energy transport by the atmospheric and oceanic circulation might also act as an independent contributor to the emergence of Arctic amplification [*Baggett et al.*, 2016; *Graversen and Burtu*, 2016; *Nummelin et al.*, 2017].

The ocean transports heat into the Arctic mainly through the Faroe-Shetland Strait of the Atlantic Ocean; the Pacific region is of secondary impor-

*Corresponding author: mikhail.latonin@niersc.spb.ru (Mikhail M. Latonin)

tance in the heat transport. Atlantic water significantly changes its characteristics on its way to the north across the Nordic Seas: due to mixing with the surrounding more fresh and colder polar water, as well as due to heat exchange between the ocean and the atmosphere. The modified Atlantic water enters the Arctic Basin of the Arctic Ocean through the Fram Strait and further spreads under the pycnocline in the form of a layer of warmer and saltier water [*Steele et al.*, 1995]. Atlantic water forms the main source of heat for the waters of the Eurasian Basin of the Arctic Ocean. Another branch of Atlantic water, entering the shallow Barents Sea, loses almost its total heat there during exchange with the atmosphere and carries little oceanic heat to neighboring regions [*Schauer et al.*, 2002; *Smedsrud et al.*, 2010]. There is evidence that transport of heat into the Arctic by the Atlantic water can be formalized and monitored through the decomposition of the seawater temperature time series into the empirical orthogonal functions for the area 50°–80°N, 50°W–20°E [*Gordeeva et al.*, 2022]. The prominence of the low-frequency climate variability in the North Atlantic region due to the combined effect of the Atlantic Multidecadal Oscillation and Atlantic Meridional Overturning Circulation is highlighted in [*Bekryaev*, 2019].

The Atlantic region is also the main corridor for the atmospheric heat transport into the Arctic. According to some estimations, half of the wintertime warming in the majority of the Arctic Ocean since the end of the 19th century can be explained by the predominantly North Atlantic storm systems carrying atmospheric sensible and latent heat [*Woods and Caballero*, 2016; *Graham et al.*, 2017; *Alekseev et al.*, 2019]. Although the dry-static energy flux dominates the net atmospheric energy transport, the latent heat flux into the Arctic might have a greater warming effect due to the positive feedback with sea ice via the enhanced downward longwave radiation [*Lee et al.*, 2017].

The role of meridional oceanic and atmospheric heat fluxes in the emergence of the Arctic amplification and in its variations in time remains poorly understood. The present study aims to derive new relationships between the interannual and decadal variability of the Arctic amplification and the coupled oceanic and atmospheric meridional heat fluxes into the Arctic. This is done from a regional perspective; therefore, the advective fluxes are estimated at the entrance to the Arctic across the "Atlantic Gate". Previous studies usually investigated the linkages between the poleward energy transport and Arctic amplification globally and considered the net energy transport. Our approach is to investigate Atlantic oceanic and atmospheric heat transport within shallow layers in the upper ocean and lower troposphere, which can have a direct influence on the surface air temperature (SAT) and Arctic amplification. This allows us to make a more precise assessment of the heat transport's influence on the Arctic amplification because this phenomenon is most pronounced near the Earth's surface. Moreover, we made joint assessment of the complex impact of the coupled atmospheric and oceanic heat fluxes on the variability of the Arctic amplification. The coupling of the heat fluxes in the ocean and atmosphere plays an important role in the observed climate tendencies. Therefore, a joint analysis of the role of these processes in the emergence of the Arctic amplification at different time scales was carried out, which made it possible to identify additional mechanisms that regulate the variability of the Arctic amplification.

2 Materials and methods

2.1 Data for the calculations and analysis

To calculate the meridional oceanic heat transport, seawater potential temperature data, salinity and meridional current velocity for different depths of the oceanic reanalysis ORAS4 were downloaded (https://icdc.cen.uni-hamburg.de/daten/reanalysis-ocean/easy-init-ocean/ecmwf-ocean-reanalysis-system-4-oras4.html). For the calculation of the meridional atmospheric heat transport, air temperature data, specific humidity and meridional wind velocity for isobaric surfaces of atmospheric reanalysis ERA5 (https://climate.copernicus.eu/climate-reanalysis) were used. Geopotential data were also downloaded from the website of ERA5 reanalysis. This variable was transformed into the geopotential heights after dividing by the gravitational acceleration (9.80665 m s^{-2}). Table 1 shows the characteristics of the reanalyses applied.

A uniform period of 1958–2017 with monthly temporal resolution was used for the analysis. To calculate Arctic amplification, monthly mean SAT data for the Northern Hemisphere were downloaded from the ERA5 reanalysis. For further analysis, the monthly mean sea level pressure data from the ERA5 reanalysis and the Arctic Ocean Oscillation (AOO) index (https://www2.whoi.edu/site/beaufortgyre/results/arctic-ocean-oscillation-index-aoo/) were used.

The AOO index was first introduced by [*Proshutinsky and Johnson*, 1997]. It is defined by the magnitude of the sea surface height horizontal gradient calculated from the simulated sea surface height field across the Arctic. This climate index is related to the conceptual model of Arctic climate variability proposed by [*Proshutinsky et al.*, 2015]. According to this model, the mechanism of

Table 1 : Reanalyses used for the calculation of heat transports

Dataset	Grid resolution	Available years	Reference
ORAS4 (ocean)	$1° \times 1°$	1958–2017	[*Balmaseda et al.*, 2013]
ERA5 (atmosphere)	$0.25° \times 0.25°$	1950–2021	[*Hersbach et al.*, 2020]

the decadal oscillation of the Arctic Ocean is self-regulated by two processes: the meridional atmospheric heat transport from the subpolar North Atlantic into the Arctic and the freshwater flux from the Arctic Ocean into the Nordic Seas. An increase in the atmospheric transport of heat and moisture into the Central Arctic leads to an increase in air temperature and an increase in cyclonic atmospheric vorticity in this region. As a result, the wind effect should lead to an increase in the freshwater flux from the Arctic Ocean into the Nordic Seas and a decrease in the surface salinity here. As a result, the stratification of the upper part of the Nordic Seas increases and winter convection weakens there, which leads to a decrease in vertical ocean–atmosphere heat fluxes and a weakening of cyclogenesis in this region. This, in turn, leads to a decrease in the atmospheric transport of heat and moisture into the Central Arctic, a decrease in air temperature there and an increase in anticyclonic vorticity. The wind effect of the anticyclonic circulation regime leads to the accumulation of freshwater in the Beaufort Gyre of the Arctic Ocean due to the intensification of the Ekman transport convergence. As a result, the freshwater flux into the Nordic Seas decreases, where, as a result, salinity increases, which contributes to the intensification of winter convection due to the weakening of the stratification of the upper ocean's layer [*Malmberg and Jónsson*, 1997; *Proshutinsky et al.*, 2002].

2.2 Selection of sections to calculate integral heat transports in the ocean and atmosphere across the "Atlantic Gate"

According to the data of the oceanic reanalysis ORAS4 and climatic reanalysis ERA5, the integral meridional heat transports across the "Atlantic Gate" in the ocean and atmosphere were calculated for the period 1958–2017. The boundaries of the sections were defined based on a condition to include only the heat transports directed predominantly northwards both in the ocean and atmosphere. The following sections were used along the latitude of 66.5°N: from −4.5°E to 13.5°E in the ocean and from −5°E to 80°E in the atmosphere (Figure 1).

The selected latitude practically corresponds to the Arctic Circle; therefore, the sections across it can be considered as the entrance to the Arctic. The oceanic section was bounded from below by the isopycnal of potential density of 27.85 kg m^{-3} [*Morgan*, 1994; *Vesman et al.*, 2020], above which, within the section under consideration (−4.5°E–13.5°E), the average transport is directed to the north (Figure 2). In the atmospheric circulation, the calculations were also bounded by the area of the section with the average heat transport to the north over the studied period: between −5°E and 80°E ("Atlantic Gate"). From above, the calculations were bounded by an isobaric surface of 800 hPa. The selection of atmospheric section is based on the study by [*Alekseev et al.*, 2019], where it was demonstrated that SAT variability in the Arctic is dominated by the atmospheric sensible and latent heat fluxes in the lower troposphere across the parallel 70°N in the Atlantic domain 0°–80°E. We have verified that it is in the 1000–800 hPa layer the average atmospheric heat transport over the period of analysis is directed mainly to the north across the "Atlantic Gate" at the latitude 66.5°N.

2.3 Calculation of integral heat transports in the ocean and atmosphere and statistical analysis

Oceanic sensible (by definition) heat transport (OSHT, W m^{-2}) was calculated using the formula (1):

$$\mathrm{OSHT}_{l,z,t(66.5°\mathrm{N})} = C_p \rho \theta_{l,z,t} V_{l,z,t}, \quad (1)$$

where C_p is the mean specific heat capacity of seawater at constant pressure equal to 4000 J $kg^{-1}K^{-1}$, ρ is the mean seawater density equal to 1028 kg m^{-3}, l is longitude, z is depth, t is time, θ is the monthly mean seawater potential temperature (K), V is the monthly mean northward current velocity (m s^{-1}).

Integral heat transport (in W) was calculated according to the equation (2):

$$\mathrm{OSHT}_{int.} = \int_{5m}^{\sigma_{27.85}} \int_{-4.5°E}^{13.5°E} (\mathrm{OSHT}_{l,z,t(66.5°N)}) dl dz, \quad (2)$$

where integration over the longitude was carried out from −4.5°E to 13.5°E with a step $dl = 1°$, and over the depth, it was carried out from 5 m to

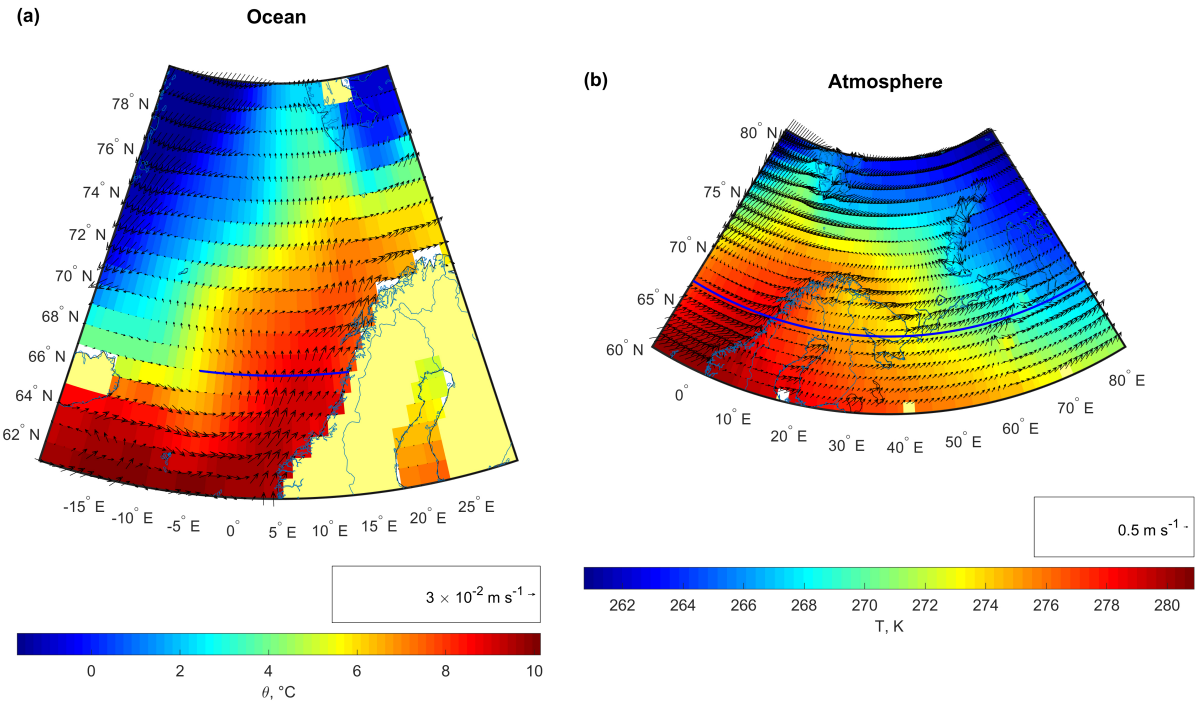

Figure 1: Average temperatures and total velocity vectors for the period 1958–2017 with monthly discreteness at a depth of 5 m in the ocean (a) and an isobaric surface of 1000 hPa in the atmosphere (b). The blue lines show the sections across which the heat transports were calculated.

depths confined by the isopycnal $\sigma = 27.85$ kg m^{-3}. Numerical integration was carried out by the trapezoidal method.

Atmospheric sensible and latent heat transports (ASHT and ALHT, W m^{-2}) were calculated using the formulas (3) and (4):

$$\mathrm{ASHT}_{l,p,t(66.5°N)} = C_p \rho T_{l,p,t} V_{l,p,t}, \quad (3)$$

$$\mathrm{ALHT}_{l,p,t(66.5°N)} = L_v \rho Q_{l,p,t} V_{l,p,t}, \quad (4)$$

where C_p is the mean specific heat capacity of air at constant pressure equal to 1005 J kg^{-1}K^{-1}, L_v is the mean latent heat of vaporization equal to 2.5 × 10^6 J kg^{-1}, ρ is the mean air density equal to 1.3 kg m^{-3}, l is longitude, p is isobaric surface, t is time, T is the monthly mean air temperature (K), Q is the monthly mean specific humidity (kg kg^{-1}), V is the monthly mean northward wind velocity (m s^{-1}).

It is more precise to assess atmospheric heat transport based on the hourly or daily data. However, a higher temporal discretization of air temperature, specific humidity and wind velocity affects the absolute values of heat transports only. The decadal variability, which is a focus of this study, is not affected. At the same time, monthly temporal resolution allows saving computational resources.

Integral heat transports (in W) were calculated according to (5) and (6):

$$\mathrm{ASHT}_{int.} = \int_{1000hPa}^{800hPa} \int_{-5°E}^{80°E} (\mathrm{ASHT}_{l,p,t(66.5°N)}) dl dp, \quad (5)$$

$$\mathrm{ALHT}_{int.} = \int_{1000hPa}^{800hPa} \int_{-5°E}^{80°E} (\mathrm{ALHT}_{l,p,t(66.5°N)}) dl dp, \quad (6)$$

where integration over the longitude was carried out from −5°E to 80°E with a step $dl = 0.25°$, and over the height, it was carried out from 1000 hPa to 800 hPa with a step $dp = 25$ hPa in accordance with the data on geopotential heights (m) at every grid point corresponding to the isobaric surfaces. Numerical integration was carried out by the trapezoidal method.

The monthly values obtained were averaged for each calendar year (January–December), and then interannual variability was analyzed. This temporal discreteness is the most significant from the climatic point of view, and the AOO index is available for the annual values only. For the integral heat transports, means, standard deviations, and Pearson correlation coefficients were calculated. The confidence intervals for the uncertainties of the means were calculated based on the

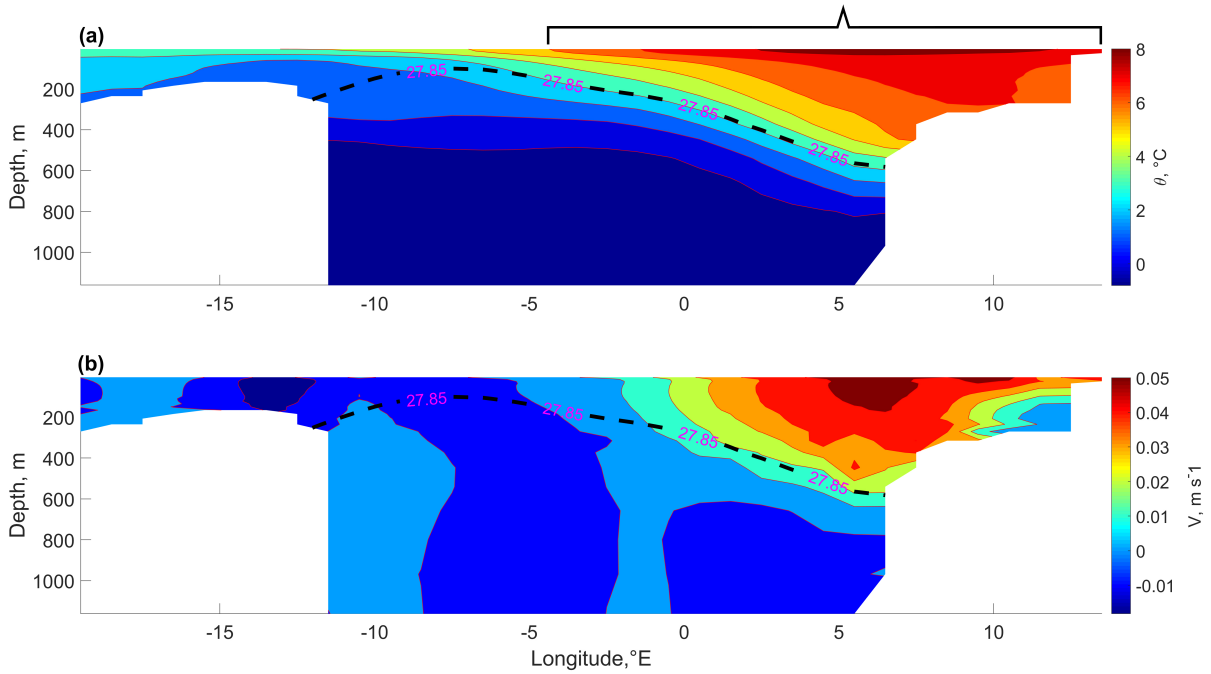

Figure 2: Zonal oceanic section across 66.5°N of the seawater potential temperature (a, °C) and of the meridional component of the current velocity (b, m s^{-1}), averaged over the period 1958–2017 according to the ORAS4 reanalysis data. The black dashed curve is the isopycnal of the potential density of 27.85 kg m^{-3} bounding the layer of Atlantic waters from below. The curly bracket shows the region used for the calculation of oceanic heat transport.

t-distribution at the 5% significance level [*Wilks*, 2006]. The presence of cycles and trends was also investigated. The statistical significance of linear trends was assessed by means of the Mann-Kendall test [*Greene et al.*, 2019]. Cycles and phase shifts were identified based on the continuous wavelet transform using the Morlet wavelet [*Torrence and Compo*, 1998; *Grinsted*, 2004; *Grinsted et al.*, 2004]. The relationship of time series in the time-frequency space was estimated using the wavelet coherence $R_n^2(s)$ in the (7). This is an analogue of coherence in spectral analysis; however, it depends not only on frequency, but also on time:

$$R_n^2(s) = \frac{|S(s^{-1} W_n^{XY}(s))|^2}{S(s^{-1}|W_n^X(s)|^2) \cdot S(s^{-1}|W_n^Y(s)|^2)}, \quad (7)$$

where S is a smoothing operator, s is a time scale, $W_n^{XY}(s)$ is the cross wavelet transform, $W_n^X(s)$ is the wavelet transform of the first time series, $W_n^Y(s)$ is the wavelet transform of the second time series.

In the wavelet coherence, the lag in years (*Lag*) of one time series relative to another was calculated by the formula (8):

$$Lag = \frac{\varphi T}{2\pi}, \quad (8)$$

where φ is a phase angle (radian), T is a period (years).

The phase angles of the wavelet coherence were taken into account not only for statistically significant regions, but also in cases where the values of the wavelet coherences exceeded 0.5. Wavelet analysis was carried out for the linearly detrended time series.

To analyze the causes of the variability of oceanic and atmospheric heat transports, composite maps of sea level pressure anomalies were constructed for the maxima and minima of oceanic heat transport. The anomalies were calculated relative to the 1961–1990 climate normal and normalized by the standard deviation for this period. The maps were plotted for the North Atlantic – Eurasia – Arctic region (30°N–90°N, −60°E–140°E).

2.4 Calculation of Arctic amplification and investigation of its relationship with meridional heat transports

The Arctic amplification was calculated from the ERA5 reanalysis data for the area 60°N–90°N with the maximum possible spatial resolution 0.25° × 0.25°. It was defined as follows: from the time series of SAT anomalies at every grid point in the Arctic region, the time series of area-weighted average SAT anomalies in the reference region of the Northern Hemisphere (0°–59.75°N) was sub-

tracted. In both regions, SAT anomalies were calculated relative to the 1961–1990 climate normal for each month, and then mean annual anomalies were found. Previous studies considered single time series of Arctic amplification obtained on the basis of average SAT anomalies both in the Arctic and reference regions [*Francis and Vavrus*, 2015; *Davy et al.*, 2018; *Latonin et al.*, 2021]. Our approach with Arctic amplification time series per grid point in the Arctic region provides an opportunity to investigate the spatial inhomogenuity of its intensity. Interannual variability was analyzed for both heat transports and Arctic amplification.

Correlation and cross-correlation analyses were used for every grid point in the Arctic region to identify areas where the Arctic amplification is associated with the heat transports entering the Arctic across the "Atlantic Gate". As heat transports into the Arctic contribute to the emergence of Arctic amplification, the relationship with a delay of the Arctic amplification relative to the heat transports was studied. Given that the Arctic amplification has a strong positive trend, the major analysis was performed for the time series with linear trends removed. This was done to assess the contribution of fluctuations in oceanic and atmospheric heat transports to the formation and variability of Arctic amplification. For the region, where statistically significant correlation coefficients were identified at the 5% significance level, a time series of the area-weighted average Arctic amplification was obtained. Subsequently, the relationship of heat transports with the Arctic amplification was estimated in the time-frequency space by means of wavelet coherence. The Butterworth low-pass filter [*Greene et al.*, 2019] with a threshold of six years was also used. Before the joint analysis of the time series of heat transports and the regional Arctic amplification, linear trends were removed from them.

For a qualitative assessment of the possible operation of the Bjerknes compensation mechanism, cross-correlation analysis was applied for both the original time series and for the time series after an application of the low-pass filter. Then, for a time lag with the maximum anti-correlation between the low-frequency variability of oceanic and atmospheric heat transports, Bjerknes compensation was calculated numerically using the method of [*van der Swaluw et al.*, 2007] (equations (9), (10), (11) and (12)):

$$|dH_{tot}| = |dH_{ocn} + dH_{atm}|, \tag{9}$$

where dH_{tot} is the total anomaly of the oceanic (dH_{ocn}) and atmospheric (dH_{atm}) heat transports relative to the full time series length. Then, the maximum anomaly of the heat transport (F) was found according to the formula:

$$F = \max(|dH_{ocn}|, |dH_{atm}|). \tag{10}$$

Subsequently, the total anomaly of heat transports was normalized by the maximum heat transport anomaly as follows:

$$N = \frac{|dH_{tot}|}{F}. \tag{11}$$

As a result, the Bjerknes compensation (BC) was estimated in % in the following way:

$$BC = (1 - N) \times 100\%. \tag{12}$$

3 Results

3.1 Integral heat transports in the ocean and atmosphere across the "Atlantic Gate"

Figure 3 shows the time series of integral heat transports in the ocean and atmosphere across the "Atlantic Gate" (66.5°N, −4.5°E–13.5°E and 66.5°N, −5°E–80°E correspondingly).

In the oceanic heat transport, a pronounced cyclicity with a period of 10–15 years is visible, which, starting from the 2000s, is replaced by higher-frequency oscillations (Figure 3a). In the atmospheric heat transports, the leading role is played by high-frequency variability (Figure 3b,c). Table 2 presents main statistical characteristics of heat transports in Figure 3.

Table 2 shows that, on average, despite the large length of the atmospheric section (Figure 1), the ocean transports 13 times more heat to the north than the atmosphere (the sum of sensible and latent heat transports). At the same time, the errors of the means for the atmospheric heat transports are comparable with the values of the means themselves, while the error of the mean for the oceanic heat transport is significantly less than the mean. This is due to the fact that in the ocean, the mean direction of the Norwegian Current to the north across the studied section is stable compared to the mean direction of the wind in the atmosphere. Therefore, in Figure 3, oceanic heat transport is always positive, whereas in the atmosphere both positive and negative heat transports are present, the latter directed southward and representing cold air outbreaks from the Arctic. The calculation results also show that the standard deviations of atmospheric heat transports are less than the standard deviation of oceanic heat transport, what is associated with a large amplitude of the 10–15-year cycle in the oceanic heat transport. However, when comparing means and standard deviations, the variability of atmospheric heat transports is much higher than that of oceanic

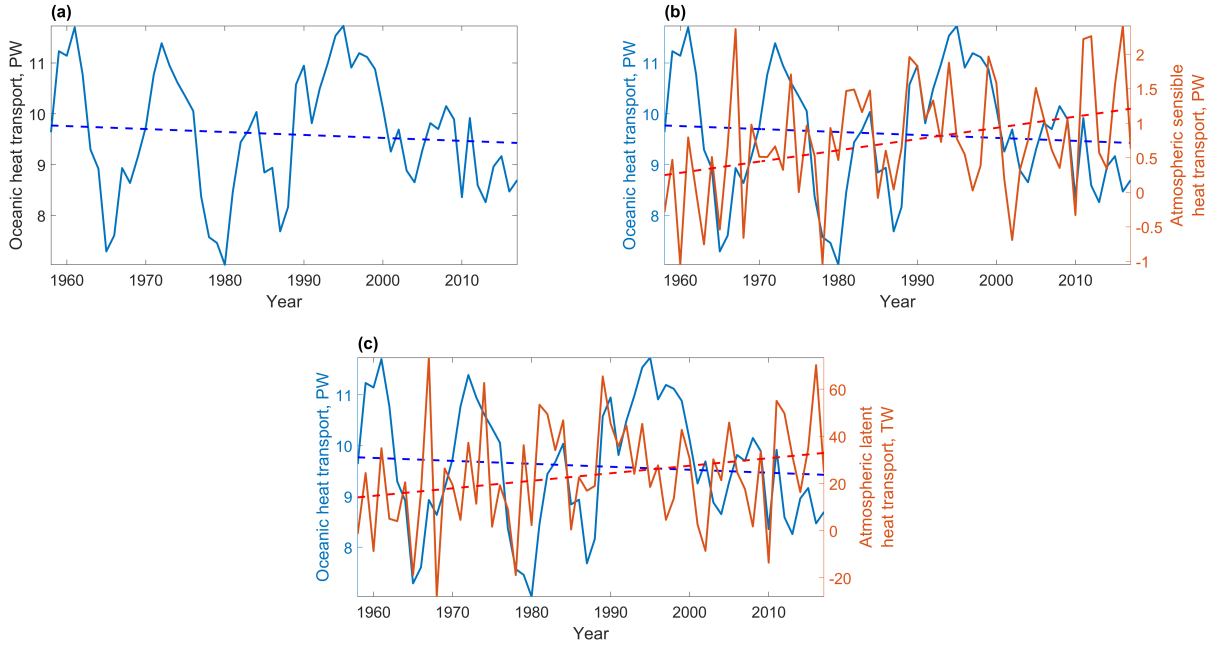

Figure 3: Meridional integral heat transports in the ocean and atmosphere at the entrance to the Atlantic sector of the Arctic. The time series of oceanic heat transport (**a**), atmospheric sensible heat transport (**b**) and atmospheric latent heat transport (**c**). Positive values correspond to the northward direction of transports. For comparison, the time series of oceanic heat transport is repeated for the panels (**b**) and (**c**). The dashed lines show linear trends.

Table 2 : Statistical characteristics of the oceanic and atmospheric heat transports across the "Atlantic Gate". The uncertainties of the means were calculated for the 5% significance level, SD is a standard deviation, k is a slope of the linear trend (statistically significant trends for the 5% significance level are in bold). R denotes the Pearson correlation coefficients between the oceanic and atmospheric sensible heat transports and between the atmospheric sensible and latent heat transports (ASHT and ALHT). The bold font indicates statistically significant correlation coefficients for the 5% significance level

	Mean (TW)	SD (TW)	k (TW/year)	R
Ocean	9600 ± 310	1210	−10	
Atmosphere (ASHT)	730 ± 220	840	**20**	0.16
Atmosphere (ALHT)	24 ± 6	23	**0.3**	**0.92**

heat transport. The correlation coefficient between the oceanic heat transport and the dominant atmospheric sensible heat transport is 0.16 (Table 2), and it is not statistically significant. This is due to the different dominant character of interannual variability of correlated heat transports. Atmospheric transports of sensible and latent heat are highly correlated with each other (R = 0.92 in Table 2). Taking into account also the fact that the sensible heat transport is several orders of magnitude higher than the latent heat transport (Table 2 and Figure 3b,c), subsequently, the atmospheric heat transport was considered as the sum of its components.

Figure 4 shows wavelet spectra and wavelet coherence of heat transports, with linear trends preliminary removed.

The wavelet spectra indicate the presence of a 10–15-year cyclicity of the oceanic heat transport for the first half of the analyzed period (1958–1985; Figure 4a). Despite the fact that the beginning of the time series is within the cone of influence, the oscillations are present here (although wavelet analysis may underestimate their amplitude; see Figure 3a). After 1985, these oscillations are also distinguished in the form of the maximum of the wavelet spectrum; however, their amplitudes can no longer be considered reliable; shorter periodicities appear. The atmospheric heat transport is characterized by higher-frequency oscillations than the oceanic one: in the 1980–1990s, 7–9-year oscillations dominate, with the period of dominant oscillations decreasing with time, giving way to a 5–7-year periodicity in the 1995–

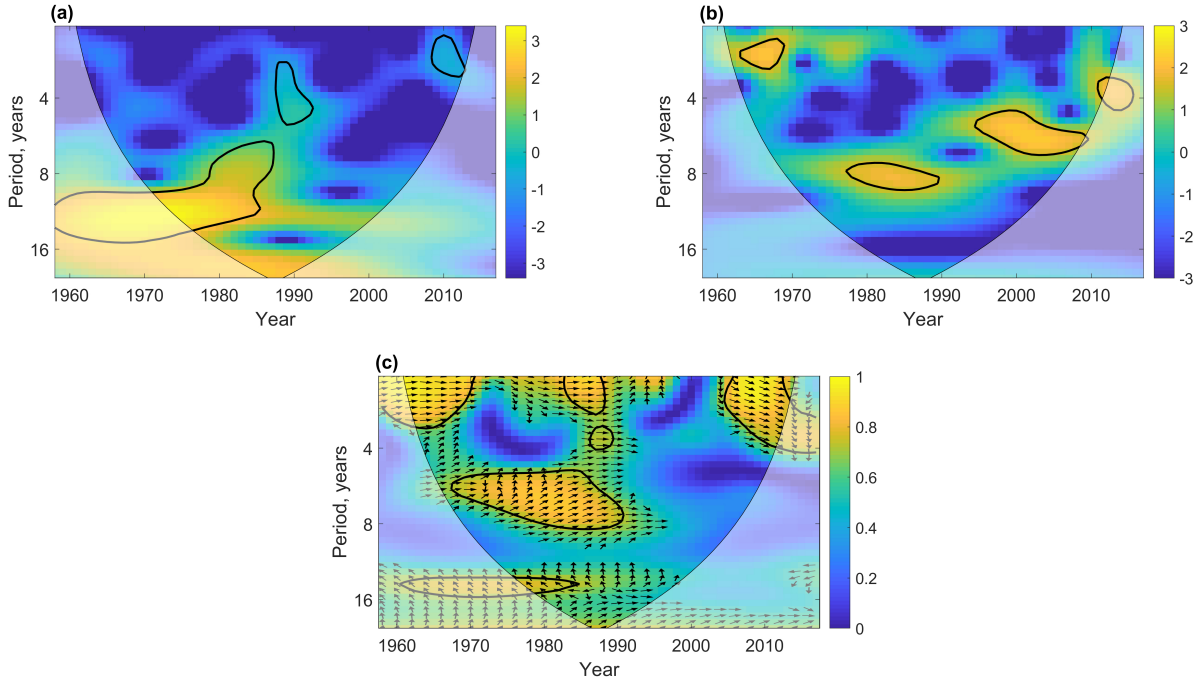

Figure 4: Wavelet power spectra of the oceanic heat transport (a), of the net (sensible and latent) atmospheric heat transport (b) and wavelet coherence between the oceanic and atmospheric heat transports (c). Wavelet power spectra (squares of wavelet amplitudes) are normalized by the variances of the original time series. Yellow areas, confined by the black curves, show significant cycles and coherences relative to the red noise spectrum at the 5% significance level. Black arrows on the panel (c) show the phase angle: directed to the right means in-phase; directed vertically upward means that the atmospheric heat transport leads the oceanic one by 90° in the given frequency band. Lighter shade areas show the cone of influence, where oscillations' amplitudes might be distorted by edge effects.

2010s and a 4-year periodicity after the 2010s (Figure 4b). Wavelet coherence (Figure 4c) indicates an episodic and predominantly in-phase relationship of the short-term variability (1–4 years) between the heat transports in the ocean and in the atmosphere. For a periodicity of 6–8 years in the 1980s, the atmosphere leads the ocean by an amount from 1/4 to 1/8 of the period. This corresponds to a lag of the oceanic heat transport relative to the atmospheric heat transport by 1–2 years (Figure 4c). This pattern of oscillations probably indicates the leading influence of the atmosphere on the ocean. For lower frequencies (periodicity of 10–15 years), oscillations in the atmospheric and oceanic heat transports are nearly anti-phase (Figure 4c), with some advance of the onset of minima/maxima in the ocean relative to significantly weaker at these frequencies maxima/minima in the atmosphere by about 2–4 years. Such a relationship may indicate a delayed ocean's impact on the atmosphere via the Bjerknes compensation mechanism on decadal time scales. For instance, the same phase shift was obtained in the study of meridional heat transports at high northern latitudes in a pre-industrial control experiment of the climate model HadCM3 [*van der Swaluw et al.*, 2007].

3.2 Relationship between variability of atmospheric and oceanic heat transports

To reveal the mechanism of formation of the detected 10–15-year oscillations in the transport of oceanic heat to the polar regions, composite maps of normalized sea level pressure anomalies were constructed separately for the episodes of the maxima (1961, 1972) and minima (1965, 1980) of oceanic heat transport. One should note that this periodicity of oscillations was most pronounced from the 1960s to the 1980s. The subsequent change in the nature of oscillations occurs at the onset of a sharp rise in the temperature of present global warming and may characterize the transition of the climate system to a new state since the late 1980s [*Reid et al.*, 2016; *Latonin et al.*, 2020b; *Sippel et al.*, 2020]. The region chosen was the North Atlantic – Eurasia – Arctic (30°–90°N, -60°E–140°E). The resulting maps are presented in Figure 5. Figure A.1 also shows the corresponding pressure fields.

The maxima in the oceanic heat transport are characterized by negative anomalies of the atmospheric pressure field over the subpolar North Atlantic (Figure 5a,c), which indicate an intensifi-

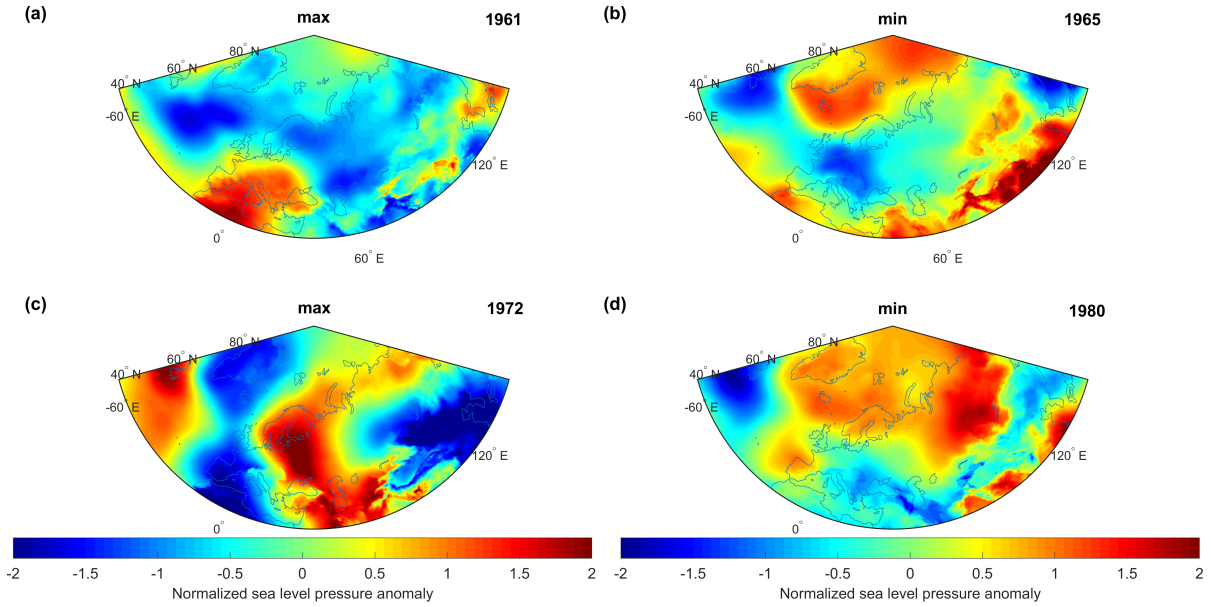

Figure 5: Composite maps of sea level pressure anomalies relative to 1961–1990 normalized by the standard deviation for this period. The maxima in the oceanic heat transport are on the left ((**a**) 1961 and (**c**) 1972), and the minima in the oceanic heat transport are on the right ((**b**) 1965 and (**d**) 1980).

cation of the Icelandic Low (Figure A.1a,c). The resulting atmospheric circulation leads to an increase in cyclonic vorticity over the Nordic Seas, which leads to an increase in the intensity of the oceanic heat transport into the Arctic.

In contrast, the minima of the oceanic heat transport are characterized by positive pressure field anomalies over the Nordic Seas and the Central Arctic (Figure 5b,d), which leads to a weakening of the Icelandic Low and an increase in anticyclonic vorticity in the Arctic (Figure A.1b,d). This should lead to a weakening of the oceanic heat transport to the north.

Thus, the maps indicate the coupling of atmospheric processes over the subpolar North Atlantic and the Central Arctic with the oceanic heat transport. The mechanism of long-term oscillation between these regions was previously proposed by [*Proshutinsky and Johnson*, 1997] and [*Proshutinsky et al.*, 2015]. It relates the transports of atmospheric heat into the Arctic and freshwater from the Arctic through a system of positive and negative feedbacks. The phase of the oscillation is determined through the AOO index, which is largely determined by the large-scale atmospheric circulation field in the Arctic [*Proshutinsky and Johnson*, 1997; *Proshutinsky et al.*, 2015]. This index shows a pronounced low-frequency oscillation of the same period, which, with the acceleration of present climate warming, has disappeared (or changed its periodicity for a longer one). Figure 6 shows the time series of oceanic and atmospheric heat transports into the Arctic along with the AOO index, as well as the wavelet coherences between them.

The results indicate that the oceanic heat transport and the AOO index do not strongly co-vary in the time-frequency space (Figure 6a,b); however, they have high common power during the 1960s–1980s in the low-frequency band corresponding to the 10–15-year cycle (Figure A.2). According to the phase angles of the wavelet coherence in (Figure 6b), during the 1960s–1980s, the variability of oceanic heat transport leads the variability of the AOO index for the periods of 10–15 years by 1.5–3 years.

There has been a long period of positive AOO index values since the late 1990s, when, over the past 20 years, the anticyclonic regime of oceanic circulation has prevailed in the Central Arctic [*Proshutinsky et al.*, 2015]. From the late 1970s to the early 1990s, the relationship between the mutual variability of the time series shifts to the region of higher frequencies corresponding to a periodicity of 5–8 years. Here, oscillations in the oceanic heat transport and the AOO become almost anti-phase, which is also clearly seen in the original time series (Figure 6a,b).

Between the AOO index and the atmospheric heat transport, a stable anti-phase relationship is observed at periods of 10–15 years throughout the entire studied period (Figure 6c). Despite the significant contribution of high-frequency variability in the atmospheric heat transport (Figure 6a), during periods of the positive phase of the AOO index (high intensity of the Beaufort Sea gyre in the Central Arctic, which corresponds to an increase in the anticyclonic atmospheric circulation over the Arctic), the heat transport from the Arctic prevails in

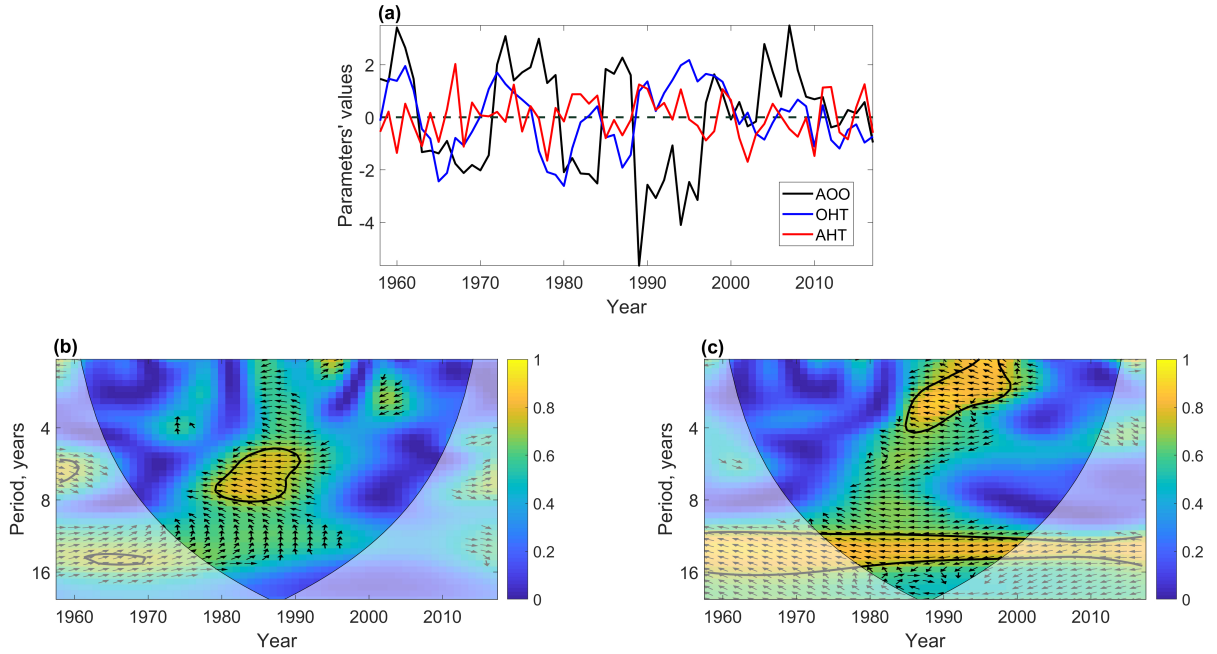

Figure 6: Time series of the AOO index, oceanic heat transport (OHT) and atmospheric heat transport (AHT) with linear trends removed (a), wavelet coherences between the AOO index and oceanic heat transport (b) and atmospheric heat transport (c). Yellow areas, confined by the black curves, show significant coherences relative to the red noise spectrum at the 5% significance level. Black arrows show the phase angle: directed to the right means in-phase and directed vertically upward means that the oceanic/atmospheric heat transport leads the AOO index by 90° in the given frequency band. Lighter shade areas on the panels (b) and (c) show the cones of influence, where oscillations' amplitudes might be distorted by edge effects.

the lower troposphere. In contrast, during periods of the negative phase of the AOO index (dominance of transpolar drift and more active removal of freshwater from the Central Arctic, which corresponds to an increase in the cyclonic atmospheric circulation over the Arctic), the heat transport into the Arctic prevails in the lower troposphere. At the same time, the weakening of the cyclicity in the AOO index after the 1990s did not lead to a loss of relationship with the atmospheric heat transport. The AOO is considered here as an indicator of the large-scale interaction of the subpolar North Atlantic and the Arctic [*Proshutinsky et al.*, 2015].

Thus, the results obtained suggest that the variability of the oceanic heat transport at the southern boundary of the Nordic Seas may act as a trigger for a change in the anticyclonic and cyclonic regimes in the Arctic. This corresponds to the concept of Bjerknes compensation when the ocean triggers changes in the atmosphere. However, [*Proshutinsky et al.*, 2015] explained the mechanism via the variability of the ocean–atmosphere heat exchange with subsequent changes of the heat transported from the Nordic Seas to the Arctic by the atmosphere. The Bjerknes compensation mechanism was not considered in [*Proshutinsky et al.*, 2015].

3.3 Relationship of meridional heat transports with Arctic amplification and Bjerknes compensation

Figure 7 shows the maps of spatial variability of correlations of interannual variability of oceanic and atmospheric heat transports (across the sections shown in Figure 1) with the mean annual Arctic amplification. The analysis was performed with the linearly detrended time series. The Arctic amplification lags from zero (a–b) to four years (i–j). Figure A.3 additionally shows the present-day mean Arctic amplification (with linear trends) calculated at every grid point of the ERA5 reanalysis as the difference between SAT anomalies in the Arctic and in the non-polar latitudes of the Northern Hemisphere.

At zero lag, the Arctic amplification is mainly associated with variability in the oceanic heat transport in the Scandinavian region (Figure 7a). However, with an increase in the time lag (up to a delay of four years), the relationship between the variability of the Arctic amplification and the variability of the oceanic heat transport across the section at 66.5°N changes sign, and its influence spreads throughout the Arctic (Figure 7c,e,g,i). The highest correlations (more than −0.6) are observed to

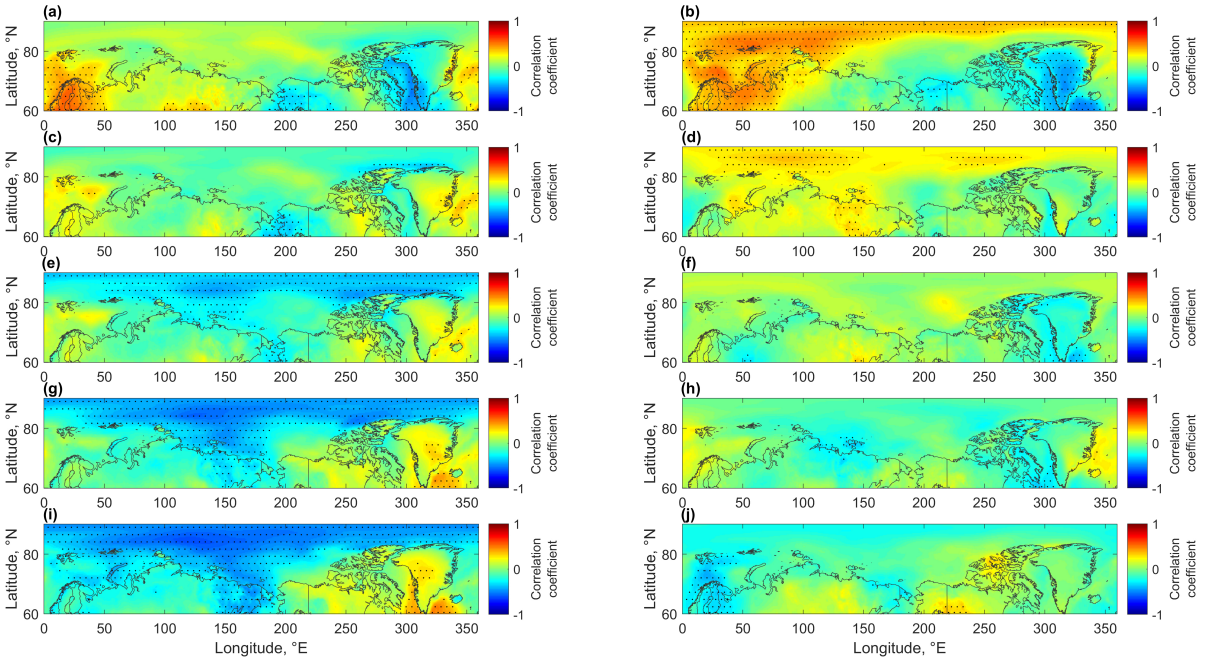

Figure 7: Correlation coefficients between the Atlantic *oceanic* heat transport at the entrance to the Arctic (across 66.5°N and −4.5°E–13.5°E) and the Arctic amplification at every grid point (*on the left*) and between the *atmospheric* heat transport at the entrance to the Arctic (across 66.5°N and −5°E–80°E) and the Arctic amplification at every grid point (*on the right*) according to the ORAS4 and ERA5 reanalyses data *with linear trends removed*. (a) and (b) are correlations with zero lag, (c) and (d) are correlations when the Arctic amplification lags by one year, (e) and (f) are correlations when the Arctic amplification lags by two years, (g) and (h) are correlations when the Arctic amplification lags by three years, and (i) and (j) are correlations when the Arctic amplification lags by four years. The black dots indicate the areas of statistically significant correlation coefficients at the 5% significance level.

the north of the Laptev Sea. At higher time lags of five years or more, the relationship weakens (not shown).

The maximum correlation coefficients between the atmospheric heat transport and the Arctic amplification are also observed north of 80°N and primarily in the Eurasian sector of the Arctic, but only with zero lag (Figure 7b). In this case, they reach 0.5 to the north of Franz Josef Land and Severnaya Zemlya. With a further delay of the Arctic amplification relative to the atmospheric heat transport, the relationship weakens and almost completely disappears for the time lag of two years or more (Figure 7f,h,j).

To identify the role of the trend in the analysis results, correlation maps were also plotted for the original time series with linear trends (Figure A.4). The results did not fundamentally change. In this case, higher correlations between the atmospheric heat transport and Arctic amplification are associated not only with the same intensity of high-frequency variability both in the atmospheric heat transport and in the Arctic amplification, but also with the same sign of the linear trend.

Despite the fact that the maximum of correlations for the ocean is shifted slightly to the east of the corresponding maximum for the atmosphere (Figure 7 and Figure A.4), a single region can be distinguished where the relationship of the Arctic amplification is high both with the oceanic heat transport and with the atmospheric heat transport. This is the region of the Eurasian Arctic (80°–90°N, 50°E–140°E), which is located to the north of the Barents, Kara and Laptev Seas. The time series of the Arctic amplification averaged over this area, together with the time series of the oceanic and atmospheric heat transports, are shown in Figure 8.

The results indicate a close relationship between the variability of the Arctic amplification and the variability of the atmospheric heat transport. This linkage is primarily in the low-frequency band: 8–15 years (Figure 8d). At the same time, the atmospheric heat transport slightly leads the Arctic amplification. The reliability of the high coherence of the atmospheric heat transport with the Arctic amplification is also confirmed in the wavelet power spectra. They show similar temporal variability of the periods of significant cyclicities of both variables in the low-frequency band (Figure A.5). It is important to note here a synchronous tendency towards a decrease in the period of oscillations with

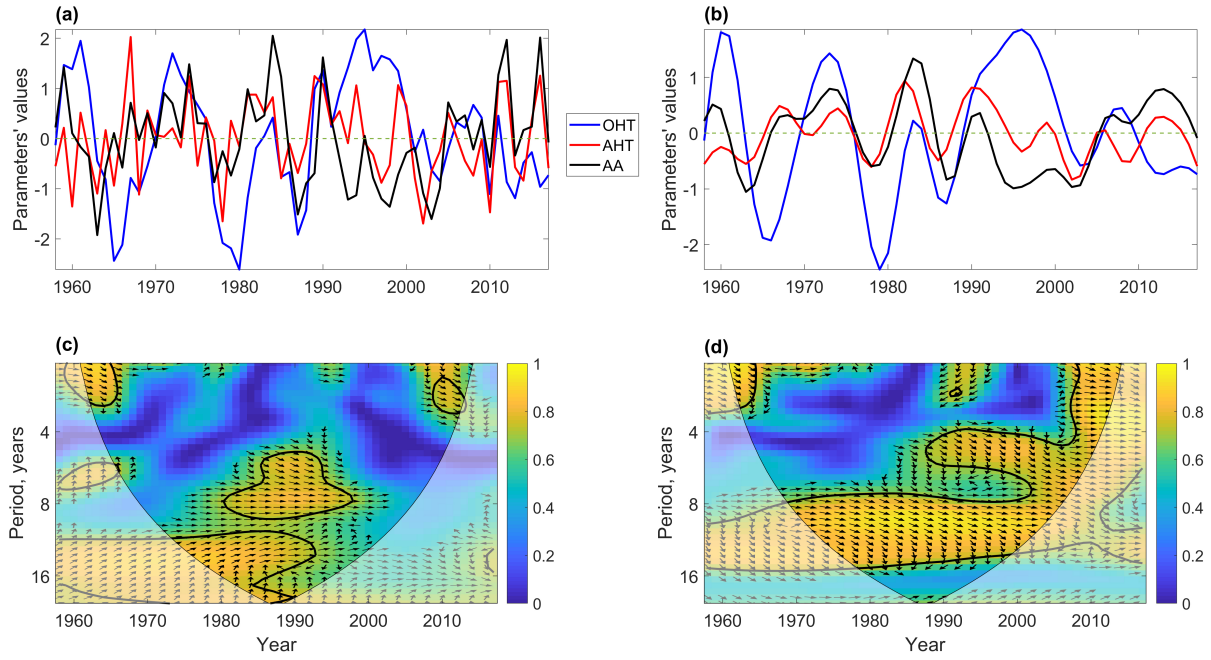

Figure 8: Time series of the oceanic heat transport (OHT), atmospheric heat transport (AHT) and regional Arctic amplification (AA) with linear trends removed (a) and after an application of the low-pass Butterworth filter with a threshold period of six years (b); wavelet coherences between the oceanic heat transport and the Arctic amplification (c) and between the atmospheric heat transport and the Arctic amplification (d). The mean annual values of the parameters of the panel (a) were used for the panels (c) and (d). Yellow areas, confined by the black curves, show significant coherences relative to the red noise spectrum at the 5% significance level. Black arrows show the phase angle: directed to the right means in-phase and directed vertically upward means that the Arctic amplification leads the oceanic/atmospheric heat transport by 90° in the given frequency band. Lighter shade areas on the panels (c) and (d) show the cones of influence, where oscillations' amplitudes might be distorted by edge effects.

time, while a close connection between the oscillations remains. This is reflected in both wavelet coherence and wavelet power spectra.

The relationship between the regional Arctic amplification and atmospheric heat transport after the removal of high-frequency oscillations (Figure 8b) shows that the maximum correlation coefficient of 0.54 occurs when the Arctic amplification lags by one year (see also Table 3). At the same time, the correlation of the time series without filtering, where the contribution of high-frequency variability dominated, showed the maximum relationship at zero time shift (Figure 7 and Figure A.4). The maximum correlation coefficient of 0.47 is observed at zero time lag for the average values of the Arctic amplification over the selected Arctic region (Figure 8a).

Table 3 shows the average wavelet coherences and phase shifts for the period with the maximum relationship of the Arctic amplification with the atmospheric heat transport at 9 years, as well as for the period of 13 years, where high correlations in the time-frequency space for the Arctic amplification are observed with both the atmospheric and oceanic heat transports.

A large band of significant and/or high wavelet coherences is observed with the oceanic heat transport as well (Figure 8c). The phase shift at low frequencies, corresponding to periods of 12–16 years, indicates a slight advance by the Arctic amplification of oscillations in the oceanic heat transport (Figure 8c; Table 3). However, according to Figure 7 and Figure A.4, it is probably more correct to interpret such a result as an advance of the maxima/minima in the oceanic heat transport of the corresponding minima/maxima (in anti-phase) of the Arctic amplification by 4–6 years. According to Figure 8b, the maximum negative correlation coefficient of −0.71 occurs when the Arctic amplification lags the oceanic heat transport by four years, similar to the time shift of the maximum correlations of the unfiltered time series in Figure 7 and Figure A.4. This anti-phase relationship is clearly visible when Figure 8 is replotted with the time series of Arctic amplification lagging by four years (Figure A.6a–b). In this case, the wavelet coherence correctly shows the anti-phase relationship between the oceanic heat transport and Arctic amplification in the low-frequency band (Figure A.6c). In contrast to the atmospheric heat

Table 3 : Numerical characteristics of the relationship of the Arctic amplification with the atmospheric and oceanic heat transports obtained on the basis of wavelet analysis (Figure 8). The values are calculated for periods of oscillations with the maximum wavelet coherence between the heat transports and the Arctic amplification. The years included in the cone of influence were omitted

	Atmospheric heat transport (9-year period, 1971–2004)	
Mean wavelet coherence	0.9	
Mean phase angle (degrees)	−26°	
Lag of Arctic amplification (years)	0.7	
	Oceanic heat transport (13-year period, 1976–1999)	Atmospheric heat transport (13-year period, 1976–1999)
Mean wavelet coherence	0.76	0.78
Mean phase angle (degrees)	18°	−79°
Lag of Arctic amplification (years)	4–6 (in anti-phase)	2.9

transport, the variability of the oceanic heat transport is predominantly low-frequency. The maximum correlation coefficient of −0.54 for the unfiltered time series averaged over the selected Arctic region (Figure 8a) is achieved when the oceanic heat transport leads the Arctic amplification by four years.

The maximum negative correlation coefficient between the low-frequency variability of the oceanic and atmospheric heat transports (Figure 8b) occurs when the latter is delayed by three years (−0.53). For the unfiltered time series (Figure 8a), the maximum relationship is observed at the same time shift, but the correlation coefficient is substantially lower (−0.29). Thus, it cannot be excluded that the significant correlation of the oceanic heat transport with the Arctic amplification, with a delay of the latter by four years, is an induced correlation arising from the anti-phase connection between the oceanic and atmospheric heat transports, the latter of which is associated with the Arctic amplification in-phase. Indeed, a negative correlation between the oceanic heat transport and the Arctic amplification would physically mean that an increase in the oceanic heat transport at the entrance to the Arctic leads to a decrease in the intensity of the Arctic amplification of the positive phase in the Eurasian Basin after four years. In reality, the magnitude of the Arctic amplification decreases one year after the atmospheric advection of heat and moisture decreases, the minimum of which occurs three years after the maximum in the oceanic heat transport.

Thus, the analysis conducted confirms the hypothesis that the ocean might be a trigger for the Arctic amplification variability affecting the atmospheric heat transport into the Arctic via the Bjerknes compensation mechanism. In turn, the atmospheric heat transport modulates the magnitude of Arctic amplification.

One should also add that, according to the observations in the Arctic Ocean, during the studied period (1958–2017), the warmth of the Atlantic waters transported by warm currents into the Arctic practically did not enter the upper mixed layer and was not directly released into the atmosphere. Only the last few years are probably an exception [*Aagaard et al.*, 1981; *Rudels*, 2015; *Ivanov et al.*, 2016; *Polyakov et al.*, 2017]. Moreover, the scale of this influence on air temperature is not yet clear. Therefore, physically, the long-term variability of the Arctic amplification can be associated with the oceanic heat transport due to the heat flux from the surface of the Nordic Seas only, from where the heat could be transported further by the atmosphere. However, Figure 7a and Figure A.4a indicate the local effect of such a direct ocean's impact on the Arctic amplification.

Figure 9 shows the time series of the oceanic heat transport anomalies for 1958–2014 and atmospheric heat transport anomalies for 1961–2017, as well as the resulting Bjerknes compensation. Anomalies were obtained with linear trends preliminary removed and after applying the Butterworth low-pass filter with a cutoff period of six years (as in Figure 8b).

Figure 9b shows that before the beginning of global warming in the 1980s, the magnitude of Bjerknes compensation was characterized by a stable oscillation with a period of about six years. After 1980, the prevailing period of oscillations increased. There are two extrema: a maximum in 1988 (99.45%) and a minimum in 1996 (18.96%). They may characterize a transition of the nature of heat exchange in polar and middle latitudes to a

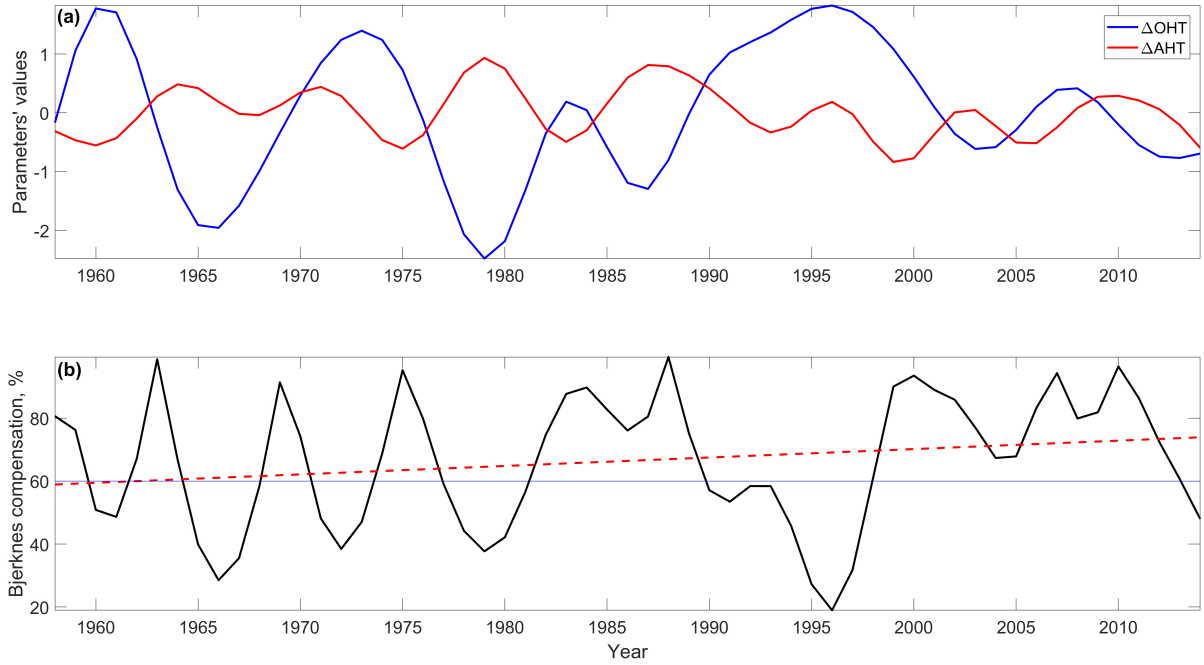

Figure 9: Low-frequency variability anomalies (according to the data of Figure 8b) of the oceanic and atmospheric heat transports (OHT and AHT correspondingly) when the ocean leads by three years (a) and the corresponding Bjerknes compensation (b). Years on the panel (a) correspond to the values of the oceanic heat transport anomalies for the period 1958–2014. The values of the atmospheric heat transport anomalies are plotted with a lag of three years (1961–2017). The Bjerknes compensation is also calculated for this time lag (12). The dashed line shows the linear trend. For the value of 60%, the reference line is added.

new state, where a regime with the high Bjerknes compensation has begun to prevail, with a significant weakening of the six-year variability.

The mean Bjerknes compensation for the entire period is 66%, which indicates a fairly high efficiency of this mechanism. This proves the validity of the proposed chain of influences of the oceanic heat transport on the atmospheric advection and of the atmospheric heat transport on the Arctic amplification.

However, atmospheric heat transport anomalies do not fully compensate oceanic heat transport anomalies. In general, the larger the anomalies in the oceanic heat transport, the less they are compensated by the atmospheric heat transport anomalies. For example, despite the pronounced anti-phase of the atmospheric and oceanic heat transports in 1979, large oceanic heat transport anomalies are observed, and the Bjerknes compensation is less than 40%.

At the same time, there is a positive statistically significant linear trend of an increase in the Bjerknes compensation magnitude by 0.3% per year, which corresponds to an increase of 15% along the trend line. Thus, in response to the climate warming, the Bjerknes compensation has begun to increase, which may indicate the tendency of the climate system to return to an equilibrium state.

4 Discussion and conclusions

The meridional heat transports in the ocean and atmosphere into the Atlantic sector of the Arctic have large differences, but are significantly interrelated at different time scales. Considering also the AOO index and the regional Arctic amplification over the Eurasian Basin of the Arctic Ocean, we conclude that there is a strong coupling between the parameters on decadal time scales (10–15-year variability).

In our study, the relationship between the AOO index and the meridional atmospheric heat transport was proved (Figure 6a,c). Whether the change in the atmospheric advection of heat and moisture into the Central Arctic is related to the winter convection dynamics in the Nordic Seas should be verified separately. For instance, for the period from 1993 to 2016 considered in the work of [*Bashmachnikov et al.*, 2021], a convection in the Greenland Sea has intensified since the 2000s. As according to the AOO index, the anticyclonic circulation regime has prevailed in the Central Arctic since 1996, associated with a decrease in the atmospheric heat transport into the Central Arctic, for the mechanism's operation proposed in [*Proshutinsky et al.*, 2015], the convection in the Nordic Seas should have weakened instead. Moreover, accord-

ing to the results of [*Bashmachnikov et al.*, 2021], the variability of the salinity of the upper part of the Greenland Sea is primarily associated not with the freshwater flux from the Arctic Ocean, but with the variability of the inflow of the Atlantic water. On the other hand, studies of winter convection in the northern part of the Norwegian Sea indicate that the intensification of convection is associated with an increase in the cyclonic vorticity over this region [*Fedorov et al.*, 2021]. However, it was found in this work that this vorticity leads to an increase in the northerly winds in the region, which leads to an increase in the convection. Whether the cyclonic vorticity anomaly itself is supported by the heat flux from the ocean, forming a positive feedback, is not clear yet.

A hypothesis about the destruction of the cyclicity in the AOO index since 1996 due to the possible contribution of freshwater, as a result of the melting of the Greenland Ice Sheet [*Proshutinsky et al.*, 2015], has also not been confirmed. A recent model study showed that Greenland's freshwater nearly does not enter the Nordic Seas, and only very small fractions of a percent can penetrate into the region from the south along with the North Atlantic Current about ten years after melted freshwater enters the ocean [*Dukhovskoy et al.*, 2019].

Nevertheless, to clarify the mechanism's operation of long-term variability in the AOO index, it is necessary to study the intensity of winter convection for all Nordic Seas and for a longer period, which would cover the changes in circulation regimes in the Central Arctic, which was stably observed until 1996. One of the difficulties for such an analysis is an insufficient coverage of the water area with oceanographic observations' data in the 20th century.

The key results of the present study are related to the dependence of Arctic amplification on the coupled oceanic and atmospheric heat fluxes. We show that the meridional atmospheric heat transport across the "Atlantic Gate" plays an important role in the variability and modulation of the intensity of the regional Arctic amplification over the Eurasian sector of the Arctic. It is important to note that here the variability of the Arctic amplification is considered both in the present period of global warming with an accelerated increase in the SAT in the Arctic (e.g., [*England et al.*, 2021]) and in the 1950s–1970s, when the SAT changes in the Arctic, middle and low latitudes did not differ substantially. According to the regionalization of the Arctic climate based on the SAT data [*Johannessen et al.*, 2016], the region of the Eurasian Arctic that we identified corresponds mainly to one of the clusters (no. 3), which covers the Arctic Ocean region north of the Kara Sea. As noted in *Johannessen et al.* [2016], this region is strongly influenced by the atmospheric transport of heat and moisture due to the penetration of extratropical cyclones from the North Atlantic, while the Atlantic water sinks here into the deeper layers of the ocean, and the heat transported by it can no longer significantly affect the SAT. This additionally confirms the above assumption that the revealed antiphase of the meridional oceanic heat transport across the "Atlantic Gate" with the regional Arctic amplification over the Eurasian Basin reflects a completely different process. Considering the results obtained in our study, with a high degree of certainty, this is a manifestation of the Bjerknes compensation mechanism [*Bjerknes*, 1964]. Bjerknes argued that with insignificant changes in the heat content of the ocean and the energy flux at the upper boundary of the atmosphere, in order to fulfill the energy conservation law, changes in the amplitudes of atmospheric and oceanic heat transports must be the same and have the opposite sign, i.e., compensate each other. *Shaffrey and Sutton* [2004] and *Shaffrey and Sutton* [2006] showed that Bjerknes compensation is effective starting from decadal time scales because with interannual variability, ocean heat content and energy flux at the upper boundary of the atmosphere change significantly. Regionally, Bjerknes compensation is most pronounced near areas where interannual sea ice area variability is significant due to the impact of oceanic heat transport [*van der Swaluw et al.*, 2007]. With an increase in the Atlantic oceanic heat transport into the Arctic, the sea surface temperature increases in the Nordic Seas, which, in turn, leads to a decrease in the meridional temperature gradient and, as a consequence, to a decrease in the meridional atmospheric pressure gradient. As a result, atmospheric heat transport into the Arctic by the synoptic eddies weakens, which forms the Bjerknes compensation [*Shaffrey and Sutton*, 2006; *Jungclaus and Koenigk*, 2010]. When investigating Bjerknes compensation at high northern latitudes, [*van der Swaluw et al.*, 2007] found that in the subpolar region of the North Atlantic, the maximum anti-correlation between the oceanic heat transport across the parallel of 70°N and the dominant component of atmospheric heat transport, represented by the moving synoptic eddies, is achieved when the atmospheric advection is delayed by 3–4 years. This result was obtained in a pre-industrial control experiment of a climate model, which indicates the fundamental nature of Bjerknes compensation as an internal mechanism of the climate system. In our paper, the maximum anti-correlation between the oceanic and atmospheric heat transports was obtained with the former leading by three years, which is in good agreement with previous studies [*van der Swaluw et al.*, 2007]. An essential role of the Bjerknes compensation mechanism in maintaining the stability

of the Earth's climate was also confirmed in the study of climatic epochs over the past 22,000 years [*Yang et al.*, 2015].

Thus, taking into account the pronounced relationship of the atmospheric heat transport with the Arctic amplification, especially in the low-frequency band with a lag of the latter by one year, the oceanic heat transport at the entrance to the Atlantic sector of the Arctic can be a predictor of the low-frequency variability of Arctic amplification over the Eurasian Basin with a lead time of four years.

Acknowledgements. This study was funded by the Ministry of Science and Higher Education of the Russian Federation under the project No. 13.2251.21.0006 (Unique Identifier RF-225121X0006; Agreement No. 075-10-2021-104 in the RF "Electronic Budget" System) and supported by the European Union's Horizon 2020 research and innovation framework programme under Grant agreement No. 101003590 (PolarRES).

References

Aagaard, K., L. Coachman, and E. Carmack (1981), On the halocline of the Arctic Ocean, *Deep Sea Research Part A. Oceanographic Research Papers*, *28*(6), 529–545, doi:https://doi.org/10.1016/0198-0149(81)90115-1.

Alekseev, G., S. Kuzmina, L. Bobylev, A. Urazgildeeva, and N. Gnatiuk (2019), Impact of atmospheric heat and moisture transport on the Arctic warming, *International Journal of Climatology*, *39*(8), 3582–3592, doi:https://doi.org/10.1002/joc.6040.

Allen, M., et al. (2018), Framing and Context, in *Global Warming of 1.5 °C: IPCC Special Report on Impacts of Global Warming of 1.5 °C above Pre-industrial Levels in Context of Strengthening Response to Climate Change, Sustainable Development, and Efforts to Eradicate Poverty*, edited by V. Masson-Delmotte, P. Zhai, H.-O. Portner, D. Roberts, J. Skea, P. Shukla, A. Pirani, W. Moufouma-Okia, C. Pean, R. Pidcock, et al., pp. 49–92, IPCC, Geneva, Switzerland, doi:10.1017/9781009157940.003.

Arrhenius, S. (1896), On the Influence of Carbonic Acid in the Air upon the Temperature of the Ground, *Lond. Edinb. Dubl. Phil. Mag*, *41*, 237–276.

Baggett, C., S. Lee, and S. Feldstein (2016), An Investigation of the Presence of Atmospheric Rivers over the North Pacific during Planetary-Scale Wave Life Cycles and Their Role in Arctic Warming, *Journal of the Atmospheric Sciences*, *73*(11), 4329–4347, doi:10.1175/JAS-D-16-0033.1.

Balmaseda, M. A., K. Mogensen, and A. T. Weaver (2013), Evaluation of the ECMWF ocean reanalysis system ORAS4, *Quarterly Journal of the Royal Meteorological Society*, *139*(674), 1132–1161, doi:https://doi.org/10.1002/qj.2063.

Bashmachnikov, I. L., A. M. Fedorov, P. A. Golubkin, A. V. Vesman, V. V. Selyuzhenok, N. V. Gnatiuk, L. P. Bobylev, K. I. Hodges, and D. S. Dukhovskoy (2021), Mechanisms of interannual variability of deep convection in the Greenland sea, *Deep Sea Research Part I: Oceanographic Research Papers*, *174*, 103,557, doi:https://doi.org/10.1016/j.dsr.2021.103557.

Bekryaev, R. V. (2019), Interrelationships of the North Atlantic multidecadal climate variability characteristics, *Russian Journal of Earth Sciences*, *19*, *ES3004*(3), 1–11, doi:10.2205/2018ES000653.

Bjerknes, J. (1964), Atlantic air-sea interaction, *Advances in Geophysics*, *10*, 1–82, doi:10.1016/S0065-2687(08)60005-9.

Bony, S., et al. (2006), How Well Do We Understand and Evaluate Climate Change Feedback Processes?, *Journal of Climate*, *19*(15), 3445–3482, doi:10.1175/JCLI3819.1.

Davy, R., L. Chen, and E. Hanna (2018), Arctic amplification metrics, *International Journal of Climatology*, *38*(12), 4384–4394, doi:https://doi.org/10.1002/joc.5675.

Dessler, A. E., Z. Zhang, and P. Yang (2008), Water-vapor climate feedback inferred from climate fluctuations, 2003–2008, *Geophysical Research Letters*, *35*(20), L20,704, doi:https://doi.org/10.1029/2008GL035333.

Dukhovskoy, D. S., I. Yashayaev, A. Proshutinsky, J. L. Bamber, I. L. Bashmachnikov, E. P. Chassignet, C. M. Lee, and A. J. Tedstone (2019), Role of Greenland Freshwater Anomaly in the Recent Freshening of the Subpolar North Atlantic, *Journal of Geophysical Research: Oceans*, *124*(5), 3333–3360, doi:https://doi.org/10.1029/2018JC014686.

England, M. R., I. Eisenman, N. J. Lutsko, and T. J. W. Wagner (2021), The Recent Emergence of Arctic Amplification, *Geophysical Research Letters*, *48*(15), e2021GL094,086, doi:10.1029/2021GL094086.

Fedorov, A. M., R. P. Raj, T. V. Belonenko, E. V. Novoselova, I. L. Bashmachnikov, J. A. Johannessen, and L. H. Pettersson (2021), Extreme Convective Events in the Lofoten Basin, *Pure and Applied Geophysics*, *178*(6), 2379–2391, doi:10.1007/s00024-021-02749-4.

Francis, J. A., and S. J. Vavrus (2015), Evidence for a wavier jet stream in response to rapid Arctic warming, *Environmental Research Letters*, *10*(1), 014,005, doi:10.1088/1748-9326/10/1/014005.

Goosse, H., et al. (2018), Quantifying climate feedbacks in polar regions, *Nat. Commun*, *9*, doi:10.1038/s41467-018-04173-0.

Gordeeva, S. M., T. V. Belonenko, and L. E. Morozova (2022), Key to the Atlantic Gates of the Arctic, *Russian Journal of Earth Sciences*, *22*, ES2004, doi:10.2205/2022ES000792.

Graham, R. M., L. Cohen, A. A. Petty, L. N. Boisvert, A. Rinke, S. R. Hudson, M. Nicolaus, and M. A. Granskog (2017), Increasing frequency and duration of Arctic winter warming events, *Geophysical Research Letters*, *44*(13), 6974–6983, doi:https://doi.org/10.1002/2017GL073395.

Graversen, R. G., and M. Burtu (2016), Arctic amplification enhanced by latent energy transport of atmospheric planetary waves, *Quarterly Journal of the Royal Meteorological Society*, *142*(698), 2046–2054, doi:https://doi.org/10.1002/qj.2802.

Graversen, R. G., P. L. Langen, and T. Mauritsen (2014), Polar Amplification in CCSM4: Contributions from the Lapse Rate and Surface Albedo Feedbacks, *Journal of Climate*, *27*(12), 4433–4450, doi:10.1175/JCLI-D-13-00551.1.

Greene, C. A., et al. (2019), The Climate Data Toolbox for MATLAB, *Geochemistry, Geophysics, Geosystems*, *20*(7), 3774–3781, doi:https://doi.org/10.1029/2019GC008392.

Grinsted, A. (2004), A cross wavelet and wavelet coherence toolbox for MATLAB, https://github.com/grinsted/wavelet-coherence, Accessed: 16 November 2020.

Grinsted, A., J. C. Moore, and S. Jevrejeva (2004), Application of the cross wavelet transform and wavelet coherence to geophysical time series, doi:10.5194/npg-11-561-2004.

Henry, M., and T. M. Merlis (2019), The Role of the Nonlinearity of the Stefan–Boltzmann Law on the Structure of Radiatively Forced Temperature Change, *Journal of Climate*, *32*(2), 335–348, doi:10.1175/JCLI-D-17-0603.1.

Hersbach, H., et al. (2020), The ERA5 global reanalysis, *Quarterly Journal of the Royal Meteorological Society*, *146*(730), 1999–2049, doi:https://doi.org/10.1002/qj.3803.

Hwang, J., Y.-S. Choi, W. Kim, H. Su, and J. H. Jiang (2018), Observational estimation of radiative feedback to surface air temperature over Northern High Latitudes, *Climate Dynamics*, *50*(1), 615–628, doi:10.1007/s00382-017-3629-6.

Ivanov, V., V. Alexeev, N. V. Koldunov, I. Repina, A. B. Sandø, L. H. Smedsrud, and A. Smirnov (2016), Arctic Ocean Heat Impact on Regional Ice Decay: A Suggested Positive Feedback, *Journal of Physical Oceanography*, *46*(5), 1437–1456, doi:10.1175/JPO-D-15-0144.1.

Johannessen, O. M., S. I. Kuzmina, L. P. Bobylev, and M. W. Miles (2016), Surface air temperature variability and trends in the Arctic: new amplification assessment and regionalisation, *Tellus A: Dynamic Meteorology and Oceanography*, *68*(1), 28,234, doi:10.3402/tellusa.v68.28234.

Jungclaus, J. H., and T. Koenigk (2010), Low-frequency variability of the arctic climate: the role of oceanic and atmospheric heat transport variations, *Climate Dynamics*, *34*(2), 265–279, doi:10.1007/s00382-009-0569-9.

Latonin, M. M., I. L. Bashmachnikov, and L. P. Bobylev (2020a), The Arctic amplification phenomenon and its driving mechanisms, *Fundam. Prikl. Gidrofiz.*, *13*, 3–19, doi:10.7868/S2073667320030016.

Latonin, M. M., V. A. Lobanov, and I. L. Bashmachnikov (2020b), Discontinuities in Wintertime Warming in Northern Europe during 1951–2016, *Climate*, *8*(6), doi:10.3390/cli8060080.

Latonin, M. M., I. L. Bashmachnikov, L. P. Bobylev, and R. Davy (2021), Multi-model ensemble mean of global climate models fails to reproduce early twentieth century Arctic warming, *Polar Science*, *30*, 100,677, doi:https://doi.org/10.1016/j.polar.2021.100677, Special Issue on "Polar Studies – Window to the changing Earth".

Lee, H. J., M. O. Kwon, S.-W. Yeh, Y.-O. Kwon, W. Park, J.-H. Park, Y. H. Kim, and M. A. Alexander (2017), Impact of Poleward Moisture Transport from the North Pacific on the Acceleration of Sea Ice Loss in the Arctic since 2002, *Journal of Climate*, *30*(17), 6757–6769, doi:10.1175/JCLI-D-16-0461.1.

Malmberg, S.-A., and S. Jónsson (1997), Timing of deep convection in the Greenland and Iceland Seas, *ICES Journal of Marine Science*, *54*(3), 300–309, doi:10.1006/jmsc.1997.0221.

Morgan, P. P. (1994), *SEAWATER: a library of MATLAB computational routines for the properties of sea water, ver. 1.2*, 37 pp., CSIRO Marine Laboratories, Hobart, Australia.

Nummelin, A., C. Li, and P. J. Hezel (2017), Connecting ocean heat transport changes from the midlatitudes to the Arctic Ocean, *Geophysical Research Letters*, *44*(4), 1899–1908, doi:https://doi.org/10.1002/2016GL071333.

Pithan, F., and T. Mauritsen (2014), Arctic amplification dominated by temperature feedbacks in contemporary climate models, *Nature Geoscience*, *7*(3), 181–184, doi:10.1038/ngeo2071.

Polyakov, I. V., et al. (2017), Greater role for Atlantic inflows on sea-ice loss in the Eurasian Basin of the Arctic Ocean, *Science*, *356*(6335), 285–291, doi:10.1126/science.aai8204.

Previdi, M., K. L. Smith, and L. M. Polvani (2021), Arctic amplification of climate change: a review of underlying mechanisms, *Environmental Research Letters*, *16*(9), 093,003, doi:10.1088/1748-9326/ac1c29.

Proshutinsky, A., R. H. Bourke, and F. A. McLaughlin (2002), The role of the Beaufort Gyre in Arctic climate variability: Seasonal to decadal climate scales, *Geophysical Research Letters*, *29*(23), 15–1–15–4, doi:https://doi.org/10.1029/2002GL015847.

Proshutinsky, A., D. Dukhovskoy, M.-L. Timmermans, R. Krishfield, and J. L. Bamber (2015), Arctic circulation regimes, *Philosophical Transactions of the Royal Society A: Mathematical, Physical and Engineering Sciences*, *373*(2052), 20140,160, doi:10.1098/rsta.2014.0160.

Proshutinsky, A. Y., and M. A. Johnson (1997), Two circulation regimes of the wind-driven Arctic Ocean, *Journal of Geophysical Research: Oceans*, *102*(C6), 12,493–12,514, doi:https://doi.org/10.1029/97JC00738.

Reid, P. C., et al. (2016), Global impacts of the 1980s regime shift, *Global Change Biology*, *22*(2), 682–703, doi:https://doi.org/10.1111/gcb.13106.

Rudels, B. (2015), Arctic Ocean circulation, processes and water masses: A description of observations and ideas with focus on the period prior to the International Polar Year 2007–2009, *Progress in Oceanography*, *132*, 22–67, doi:https://doi.org/10.1016/j.pocean.2013.11.006, Oceanography of the Arctic and North Atlantic Basins.

Schauer, U., H. Loeng, B. Rudels, V. K. Ozhigin, and W. Dieck (2002), Atlantic Water flow through the Barents and Kara Seas, *Deep Sea Research Part I: Oceanographic Research Papers*, *49*(12), 2281–2298, doi:https://doi.org/10.1016/S0967-0637(02)00125-5.

Screen, J. A., and I. Simmonds (2010), The central role of diminishing sea ice in recent Arctic temperature amplification, *Nature*, *464*(7293), 1334–1337, doi:10.1038/nature09051.

Serreze, M. C., and R. G. Barry (2011), Processes and impacts of Arctic amplification: A research synthesis, *Global and Planetary Change*, *77*(1), 85–96, doi:https://doi.org/10.1016/j.gloplacha.2011.03.004.

Serreze, M. C., and J. A. Francis (2006), The Arctic Amplification Debate, *Climatic Change*, *76*(3), 241–264, doi:10.1007/s10584-005-9017-y.

Shaffrey, L., and R. Sutton (2004), The Interannual Variability of Energy Transports within and over the Atlantic Ocean in a Coupled Climate Model, *Journal of Climate*, *17*(7), 1433–1448, doi:10.1175/1520-0442(2004)017<1433:TIVOET>2.0.CO;2.

Shaffrey, L., and R. Sutton (2006), Bjerknes Compensation and the Decadal Variability of the Energy Transports in a Coupled Climate Model, *Journal of Climate*, *19*(7), 1167–1181, doi:10.1175/JCLI3652.1.

Sippel, S., E. M. Fischer, S. C. Scherrer, N. Meinshausen, and R. Knutti (2020), Late 1980s abrupt cold season temperature change in Europe consistent with circulation variability and long-term warming, *Environmental Research Letters*, *15*(9), 094,056, doi:10.1088/1748-9326/ab86f2.

Smedsrud, L. H., R. Ingvaldsen, J. E. Ø. Nilsen, and Ø. Skagseth (2010), Heat in the Barents Sea: transport, storage, and surface fluxes, *Ocean Science*, *6*(1), 219–234, doi:10.5194/os-6-219-2010.

Steele, M., J. H. Morison, and T. B. Curtin (1995), Halocline water formation in the Barents Sea, *Journal of Geophysical Research: Oceans*, *100*(C1), 881–894, doi:https://doi.org/10.1029/94JC02310.

Torrence, C., and G. P. Compo (1998), A Practical Guide to Wavelet Analysis, *Bulletin of the American Meteorological Society*, *79*(1), 61–78, doi:10.1175/1520-0477(1998)079<0061:APGTWA>2.0.CO;2.

van der Swaluw, E., S. S. Drijfhout, and W. Hazeleger (2007), Bjerknes Compensation at High Northern Latitudes: The Ocean Forcing the Atmosphere, *Journal of Climate*, *20*(24), 6023–6032, doi:10.1175/2007JCLI1562.1.

Vesman, A. V., I. L. Bashmachnikov, P. A. Golubkin, and R. P. Raj (2020), The coherence of the oceanic heat transport through the Nordic seas: oceanic heat budget and interannual variability, *Ocean Science Discussions*, *2020*, 1–24, doi:10.5194/os-2020-109.

Volodin, E., V. Galin, N. Diansky, V. Dymnikov, and V. Lykossov (2008), Mathematical modeling of potential catastrophic climate changes, *Russ. J. Earth Sci*, *10*, *ES2004*, doi:10.2205/2007ES000231.

Wilks, D. S. (2006), *Statistical methods in the atmospheric sciences*, *International Geophysics Series*, vol. 91, 2nd ed., 649 pp., Elsevier Academic Press, San Diego, CA, USA.

Woods, C., and R. Caballero (2016), The Role of Moist Intrusions in Winter Arctic Warming and Sea Ice Decline, *Journal of Climate*, *29*(12), 4473–4485, doi:10.1175/JCLI-D-15-0773.1.

Yang, H., Y. Zhao, Z. Liu, Q. Li, F. He, and Q. Zhang (2015), Heat transport compensation in atmosphere and ocean over the past 22,000 years, *Scientific Reports*, *5*(1), 16,661, doi:10.1038/srep16661.

Zelinka, M. D., and D. L. Hartmann (2012), Climate Feedbacks and Their Implications for Poleward Energy Flux Changes in a Warming Climate, *Journal of Climate*, *25*(2), 608–624, doi:10.1175/JCLI-D-11-00096.1.

A Appendix

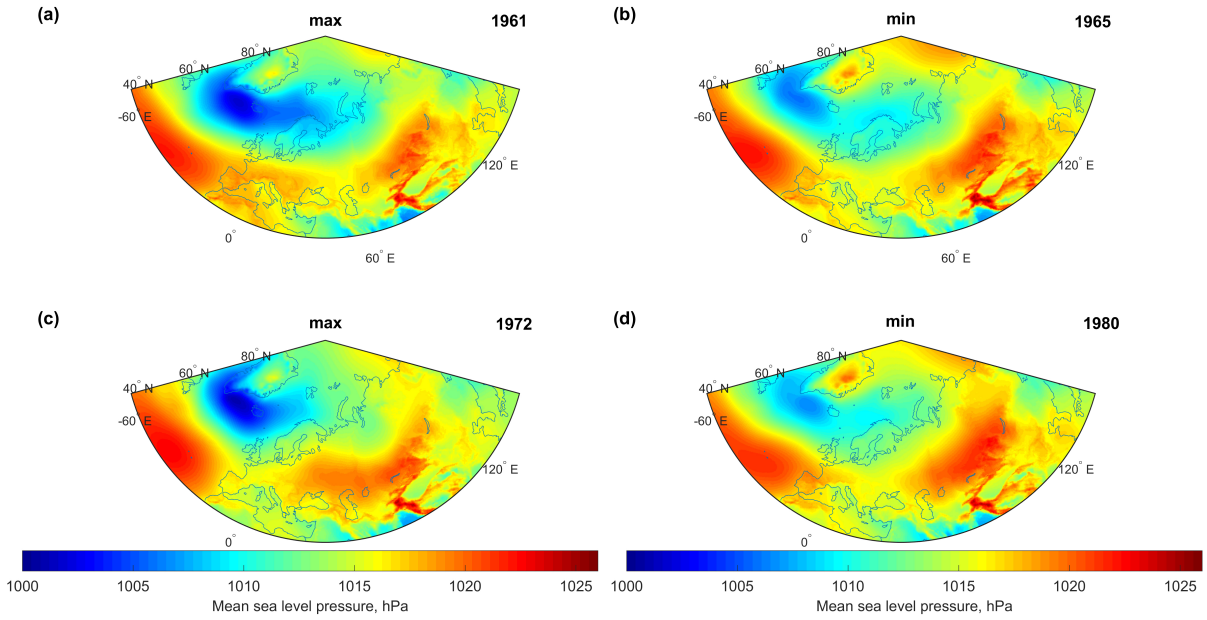

Figure A.1: Composite maps of mean sea level pressure. The maxima in the oceanic heat transport are on the left ((a) 1961 and (c) 1972), and the minima in the oceanic heat transport are on the right ((b) 1965 and (d) 1980).

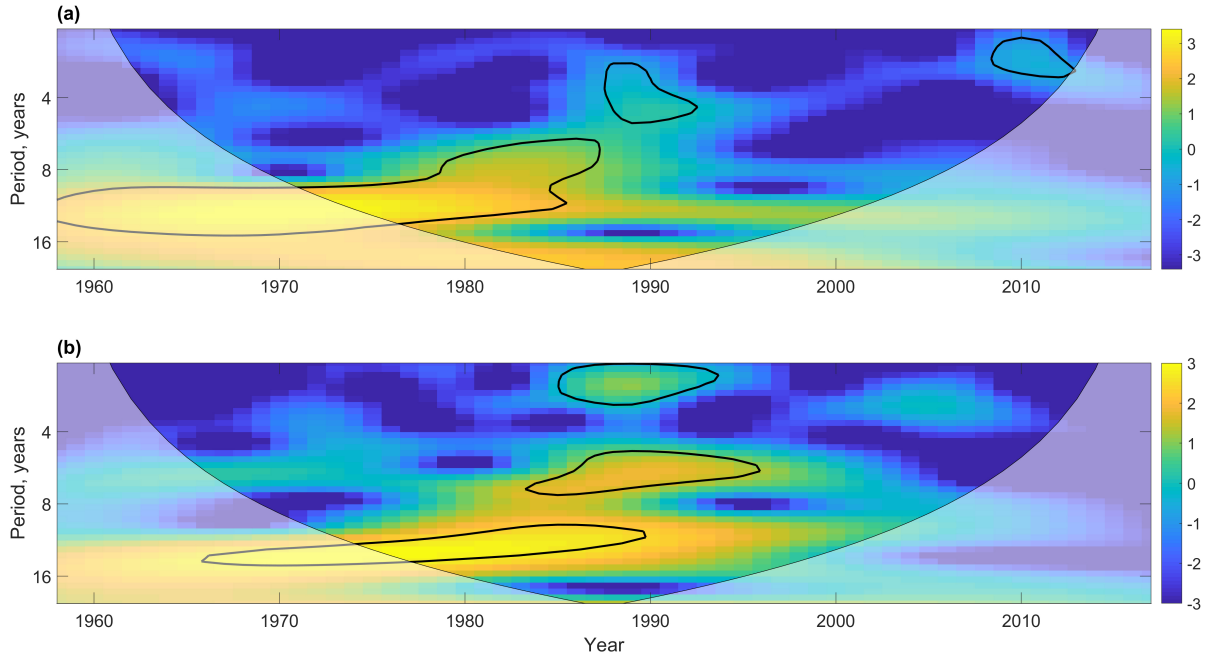

Figure A.2: Wavelet power spectra of the oceanic heat transport (a) and of the AOO index (b). Wavelet power spectra (squares of wavelet amplitudes) are normalized by the variances of the original time series. Yellow areas, confined by the black curves, show significant cycles relative to the red noise spectrum at the 5% significance level. Lighter shade areas show the cone of influence, where oscillations' amplitudes might be distorted by edge effects.

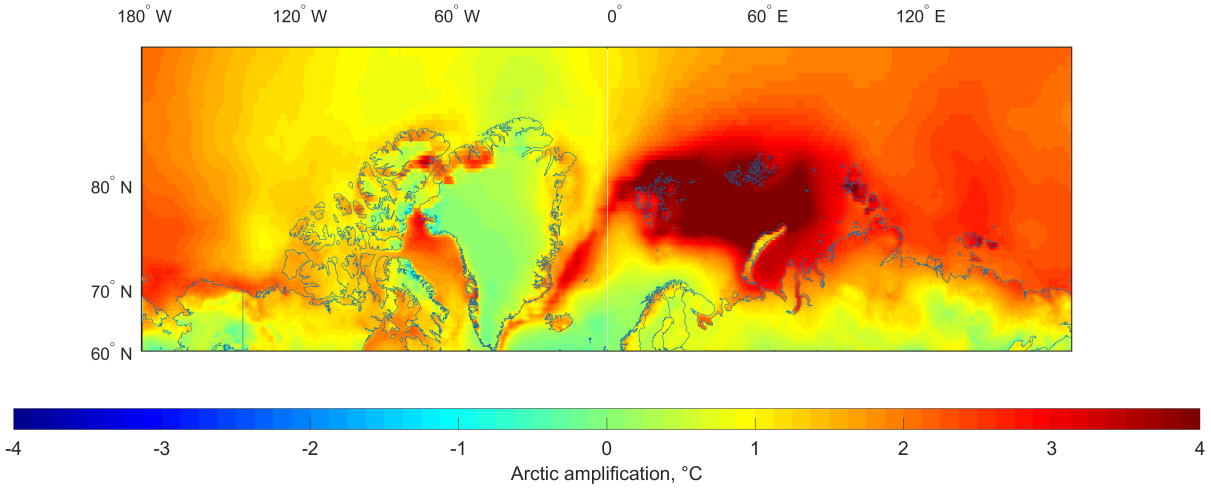

Figure A.3: Mean annual Arctic amplification calculated at every grid point according to the ERA5 reanalysis. The present period is shown with averaging for 2006–2017. Mercator map projection is used.

According to Figure A.3, the current Arctic amplification occurs mainly north of 70°N. Figure A.3 also shows important regional features of the intensity of the Arctic amplification. The rate of SAT increase is much higher in the Eastern Hemisphere than in the Western Hemisphere. The maximum intensity of the Arctic amplification is observed in the northern part of the Barents and Kara Seas and in the adjacent areas of the Arctic Ocean, between Spitsbergen and Severnaya Zemlya in the latitudinal range 75°N–82°N (Figure A.3.).

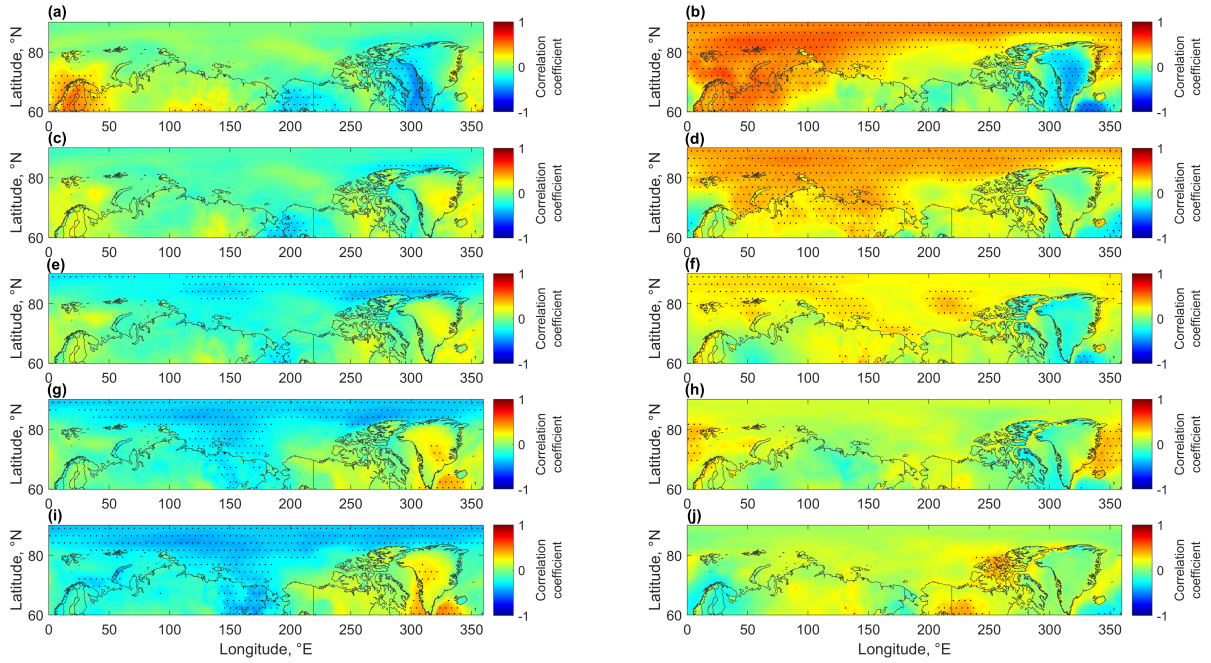

Figure A.4: Correlation coefficients between the Atlantic *oceanic* heat transport at the entrance to the Arctic (across 66.5°N and −4.5°E–13.5°E) and the Arctic amplification at every grid point (*on the left*) and between the *atmospheric* heat transport at the entrance to the Arctic (across 66.5°N and −5°E–80°E) and the Arctic amplification at every grid point (*on the right*) according to the ORAS4 and ERA5 reanalyses data. (a) and (b) are correlations with zero lag, (c) and (d) are correlations when the Arctic amplification lags by one year, (e) and (f) are correlations when the Arctic amplification lags by two years, (g) and (h) are correlations when the Arctic amplification lags by three years, and (i) and (j) are correlations when the Arctic amplification lags by four years. The black dots indicate the areas of statistically significant correlation coefficients at the 5% significance level.

In Figure A.4i, the highest correlations (−0.45) between the oceanic heat transport and Arctic amplification are observed to the north of the Laptev Sea. In Figure A.4b, the maximum correlation coefficients (0.6) between the atmospheric heat transport and the Arctic amplification are observed to the north of Franz Josef Land and Severnaya Zemlya.

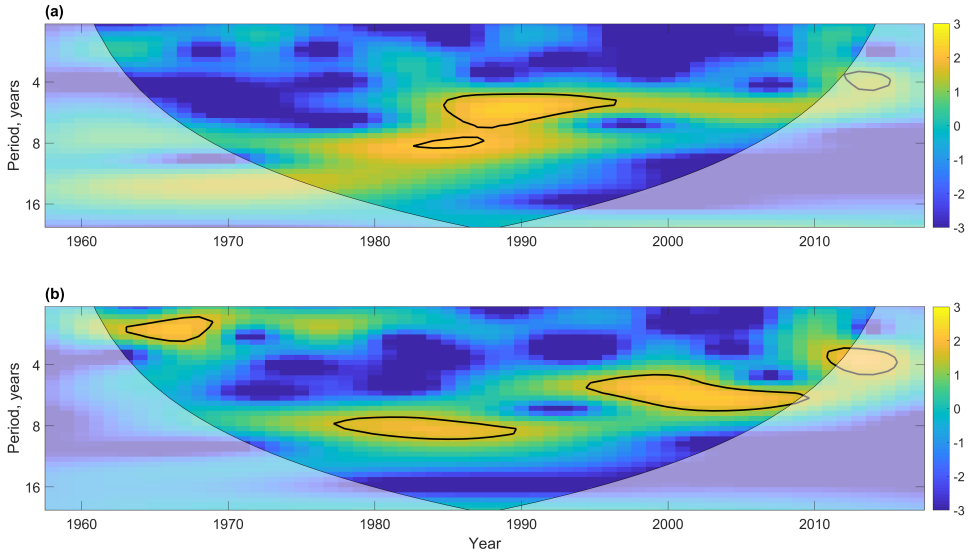

Figure A.5: Wavelet power spectra of the regional Arctic amplification (a) and the net (sensible and latent) atmospheric heat transport (b). Wavelet power spectra (squares of wavelet amplitudes) are normalized by the variances of the original time series. Yellow areas, confined by the black curves, show significant cycles relative to the red noise spectrum at the 5% significance level. Lighter shade areas show the cone of influence, where oscillations' amplitudes might be distorted by edge effects.

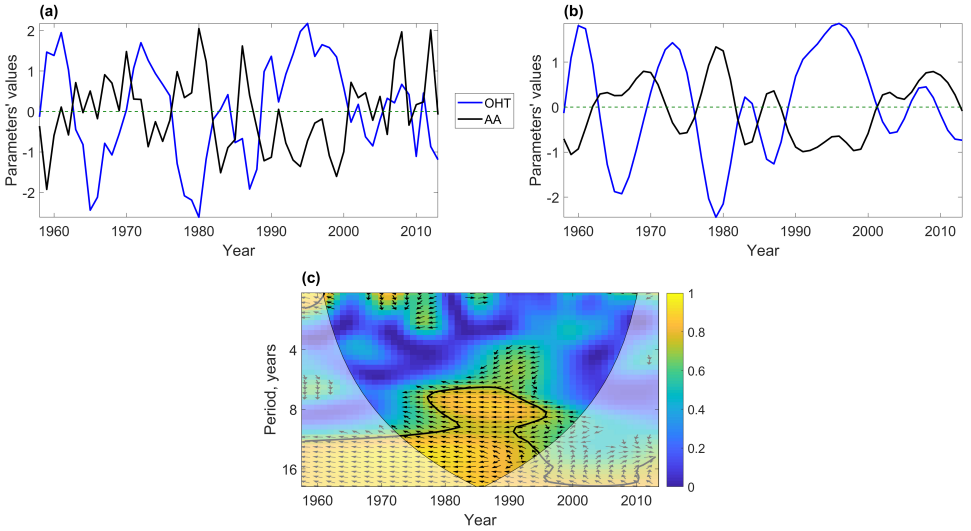

Figure A.6: Time series of the oceanic heat transport (OHT) for the period 1958–2013 and regional Arctic amplification (AA) for the period 1962–2017 with linear trends removed (a) and after an application of the low-pass Butterworth filter with a threshold period of six years (b); wavelet coherence between the oceanic heat transport and the Arctic amplification with the latter lagging by four years (c). The mean annual values of the parameters of the panel (a) were used for the panel (c). Yellow areas, confined by the black curves, show significant coherences relative to the red noise spectrum at the 5% significance level. Black arrows show the phase angle: directed to the right means in-phase and directed vertically upward means that the Arctic amplification leads the oceanic heat transport by 90° in the given frequency band. Lighter shade areas on the panel (c) show the cone of influence, where oscillations' amplitudes might be distorted by edge effects.